

THESIS FOR THE DEGREE OF LICENTIATE OF ENGINEERING

**Data-Driven Models and Correlation Strategies for
Thermal Cracking of Polymeric Feedstocks in Dual
Fluidized Beds**

RENESTEBAN FORERO FRANCO

Department of Space Earth and Environment

CHALMERS UNIVERSITY OF TECHNOLOGY

Göteborg, Sweden 2024

Data-Driven Models and Correlation Strategies for Thermal Cracking of Polymeric Feedstocks in Dual Fluidized Beds

RENESTEBAN FORERO FRANCO

© RENESTEBAN FORERO FRANCO, 2024

Department of Space Earth and Environment
Chalmers University of Technology
SE-412 96 Gothenburg
Sweden
Telephone +46 (0) 31-772 1432

Printed by Chalmers Reproservice
Gothenburg, Sweden 2024

Data-Driven Models and Correlation Strategies for Thermal Cracking of Polymeric Feedstocks in Dual Fluidized Beds

RENESTEBAN FORERO FRANCO
Division of Energy Technology
Department of Space Earth and Environment
Chalmers University of Technology

Abstract

The escalating global production and consumption of plastics pose a significant environmental threat, demanding innovative waste management solutions. Among the different kinds of recycling technologies, steam cracking is a promising alternative to mechanical recycling that allows the processing of highly heterogeneous plastic waste streams to recover the carbon into monomeric species that can be used to produce polymeric materials of virgin quality.

The product species obtained from the steam cracking comprise different kinds of molecules which include syngas, aliphatics, aromatics and soot. The distribution of species is intrinsically linked to both the reactor's operational conditions and the chemical characteristics of the feedstock. From a data analysis perspective, this distribution holds valuable information that can be leveraged for instrument validation, prediction of unmeasured species, and estimation of relevant process variables. However, this aspect often receives insufficient attention in the technology's related studies. This thesis aims to contribute to the theoretical and practical understanding of steam pyrolysis, offering validated data-driven models that can serve as tools for optimizing pyrolysis processes and for gaining insights into the relationship between feedstock characteristics and pyrolysis outcomes. The research encompasses the development and validation of two data-driven models, aimed at enhancing data quality and improving the understanding of product species distribution from steam cracking processes.

Experiments were performed with different types of plastic feedstocks in a dual fluidized bed (DFB) plant with a semi-industrial scale bubbling fluidized bed cracking reactor that was coupled with a circulating fluidized bed combustor running on biomass. The analytical setup included a Solid Phase Adsorption (SPA) method for aromatic fraction collection and a High-Temperature Reactor (HTR) for complete reforming of the hydrocarbons to syngas, which allowed estimation of the char yield. The characterization of the produced chemical species was performed with gas chromatography using thermal conductivity (TCD), flame ionization (FID) and vacuum ultraviolet (VUV).

The first part of the work encompasses the introduction of a Parametric System Model (PSM), designed for data quality assessment. This model leverages the constraints imposed by the conservation laws and the chemical nature of steam pyrolysis to ensure physically and statistically meaningful results for the product species distribution obtained from the cracking process. Special focus is placed on the conceptualization, mathematical foundation, and experimental validation of the model. In the second part of the work, the influence of feedstock polymeric composition on the product distribution is examined through the species distribution data obtained from the cracking in the DFB system of heterogeneous mixtures that originated from the rejected materials of different industrial recycling processes. The study presents a novel carbon classification framework that aids in identifying correlations between the feedstock chemical structures and the cracking products.

This study encapsulates efforts towards creating generalizable data analysis frameworks that can be used as tools for predictive analysis between the composition of polymeric mixture feedstocks and the resulting product species from steam cracking in dual fluidized beds.

Keywords: Steam Cracking, Plastic Waste Recycling, Fluidized Bed, Modelling, Numerical Estimation.

List of Publications Included in this Thesis

This thesis is based on the following papers, which can be found in the appendix of this work. The papers are referred to in the text using Roman numerals.

Paper I

Renesteban Forero-Franco, Teresa Berdugo-Vilches, Chahat Mandviwala, Martin Seemann, Henrik Thunman

Developing a Parametric System Model to describe the Product Distribution of Steam Pyrolysis in a Dual Fluidized Bed,

Fuel, Volume 348, 2023, 128518, ISSN 0016-2361, <https://doi.org/10.1016/j.fuel.2023.128518>.

Paper II

Renesteban Forero-Franco, Isabel Cañete-Vela, Teresa Berdugo-Vilches, Judith González-Arias, Jelena Maric, Henrik Thunman, Martin Seemann,

Correlations between product distribution and feedstock composition in thermal cracking processes for mixed plastic waste,

Fuel, Volume 341, 2023, 127660, ISSN 0016-2361, <https://doi.org/10.1016/j.fuel.2023.127660>.

Paper III

Chahat Mandviwala, Renesteban Forero Franco, Ivan Gogolev, Judith González-Arias, Teresa Berdugo Vilches, Isabel Cañete Cañete Vela, Henrik Thunman, Martin Seemann,

Method development and evaluation of product gas mixture from a semi-industrial scale fluidized bed steam cracker with GC-VUV,

Fuel Processing Technology, Volume 253, 2024, 108030, ISSN 0378-3820,

<https://doi.org/10.1016/j.fuproc.2023.108030>.

Publication not included in this thesis:

Judith González-Arias, Renesteban Forero-Franco, Chahat Mandviwala, Martin Seemann,
Steam gasification as a viable solution for converting single-use medical items into chemical building blocks with high yields for the plastic industry,

Resources, Conservation and Recycling, Volume 201, 2024, 107342, ISSN 0921-3449,

<https://doi.org/10.1016/j.resconrec.2023.107342>.

Contributions Report:

Paper I. Renesteban Forero Franco is the corresponding author, with responsibility for the model conceptualization, data curation, formal analysis and writing of the paper; Teresa Verdugo contributed with editing, ideas and discussion regarding the manuscript, and planning of the experimental work. Chahat Mandviwala contributed to the execution of the experimental work; Martin Seemann contributed with ideas and discussion during the preparation of the manuscript; Henrik Thunman contributed with ideas and discussion regarding the model formulation and preparation of the manuscript.

Paper II. Renesteban Forero Franco is the corresponding author, with responsibility for the model conceptualization, data curation, formal analysis and writing of the paper; Isabel Cañete Vela contributed with the planning and execution of the experimental work, as well as preliminary ideas and editing for the final version of the manuscript; Teresa Verdugo contributed with editing, ideas and discussion regarding the manuscript and the planning of the experimental work; Judith Gonzales Arias contributed with ideas and evaluation of the experimental data; Jelena Maric contributed to the execution of the experimental work; Henrik Thunman contributed with discussions and editing of the manuscript. Martin Seemann contributed ideas and discussions regarding the model formulation and preparation of the manuscript.

Paper III. Chahat Mandviwala is a corresponding co-author with responsibility for the writing and conceptualization of the manuscript, as well as the planning and execution of the experimental work; Renesteban Forero Franco is a corresponding co-author, with responsibility for the manuscript conceptualization and editing, and data curation, as well as the planning and execution of the experimental work; Ivan Gogolev, Judith Gonzales Arias and Isabel Cañete Vela contributed to the execution of the experimental work; Teresa Verdugo contributed with editing of the manuscript and planning of the experimental work; Henrik Thunman and Martin Seemann contributed with ideas, discussions and editing of the manuscript.

Table of Contents

Abstract.....	i
List of Publications Included in this Thesis.....	ii
Contributions Report:.....	iii
1. Introduction.....	1
1.1. Aim and Scope.....	4
1.2. Publication’s Contribution.....	4
2. Parametric system model development for data quality analysis.....	5
2.1. Model Formulation and Description.....	5
2.2. Model Implementation and Additional Constraints.....	7
2.3. Validation Method.....	10
3. Unraveling Correlations between the Steam Pyrolysis Product Distribution and Polymer Composition.....	13
3.1. Polymeric composition estimation method for unknown plastic mixtures.....	14
3.2. Carbon bond-based classification system model.....	17
4. Experimental Setup.....	19
4.1. Materials and Process Conditions.....	21
5. Results and Analysis.....	23
5.1. Parametric System Model Evaluation.....	23
5.2. Parametric System Model Validation and Data Quality Assessment.....	25
5.3. Correlations between Product Distribution and Feedstock: Polymeric Composition Estimations.....	26
5.4. Correlations between Product Distribution and Feedstock: Carbon Bond-Based Classification Evaluation.....	28
6. Future Research Perspectives.....	33
7. Conclusions.....	35
8. References.....	37

1. Introduction

Plastics have undoubtedly revolutionized modern living. Lightweight, versatile, and relatively cheap, they have become an integral part of our daily lives. Nonetheless, the exponential growth in the production and consumption of plastics has led to a global crisis that threatens the environment, human health, and ecosystems. Plastics production has skyrocketed over the past few decades. According to the Organization for Economic Cooperation and Development (OECD), global production levels of plastics and fibers reached a staggering 460 million metric tons (Mt) in Year 2019, with this number projected to double by Year 2050 if the current trend continues [1]. However, the plastics economy is far from circular. Around 353 Mt of plastic waste were produced worldwide in Year 2019, with 63% corresponding to short-lived products with a lifespan of less than 5 years, such as packaging (40%), consumer products (12%), and textiles (11%) [1,2]. In terms of waste management, only 15% of the plastic waste is collected for recycling, of which 40% is disposed as residue, thereby reducing the effective recycling rate to 9%. Of the remaining 91% of plastic waste, 50% is disposed of in sanitary landfills, 19% is incinerated, and a staggering 22% is mismanaged waste that is burned in open pits or thrown away in unregulated dumpsites or aquatic ecosystems [3].

Different plastic recycling techniques have been developed over the past decades, with mechanical recycling being the most-common approach. This process involves the re-melting and shaping of plastics for reuse. However, mechanical recycling is considered highly selective due to the strict requirements attached to homogeneous and uncontaminated plastic feedstocks. Thus, several sorting steps are usually needed when dealing with heterogeneous feedstocks, which reduce the energy efficiency of the overall recycling process. The effectiveness is also hindered by the progressive loss of material quality for each recycling process cycle. As a result, a large portion of the collected plastic waste may need to be recycled through a more-general recycling route, such as combustion in combination with carbon capture and utilization (CCU) technologies [4,5] for chemical synthesis, although this way comes with a significant energy cost.

Alternatively, the chemical recycling approach to plastic waste management offers the potential to convert a wide range of mixed waste materials into high-quality feedstocks for the chemical industry. Unlike mechanical recycling, which focuses on the physical properties of the plastics, chemical recycling deals with their chemical compositions. The primary goal of chemical recycling is the transformation of plastics back into their fundamental chemical building blocks — monomers. These monomers serve as the raw materials for the production of virgin plastics and various other high-quality chemical products. Solvolysis and pyrolysis are the two most-prominent methods for chemical recycling. Solvolysis involves the chemical degradation of polymers using solvents, while pyrolysis relies on the use of high temperatures in an oxygen-free environment to break down the polymer chains through free radical reactions. In the global context, chemical recycling can be seen as complementary to mechanical recycling, with the potential to process mixed or contaminated plastics at the industrial scale [6,7].

Among the technologies that are based on pyrolysis, high-temperature steam pyrolysis is of special interest due to its ability to handle heterogeneous feedstocks while minimizing the thermodynamic penalty associated with the combustion-based recycling route [6]. Falling within the general recycling category, this process, which is also known as *steam cracking*, involves subjecting carbon-based feedstocks to extreme temperatures, typically around 800°C, in the presence of steam, which acts as a quasi-inert dilution agent. The conversion process leads to the generation of a gas mixture, technically known as *producer gas*, which contains a variety of chemical species, including H₂, CO, CO₂, and various hydrocarbons in the forms of paraffins, olefins, and aromatics. In general, the species

distribution of the producer gas is intimately linked to the cracking reactor conditions and the chemical characteristics of the feedstock. This process constitutes the core of the research presented in this thesis.

The endothermic nature of pyrolysis reactions implies the addition of heat to the reaction environment, and the product distribution benefits from a steep heating gradient and controlled maximum temperature. Therefore, the choices related to reactor type and design play pivotal roles in polymer conversion and the distribution of product species. Dual Fluidized Beds (DFBs) fulfill the abovementioned requirements due to their allothermal heat supply, efficient heat transfer capabilities, and mixing characteristics. The general versatility of DFBs in terms of feedstock size and state, ash content and temperature adaptability make them well-suited to enhancing the robustness of the recycling process for different feedstocks and is the technology used in this work. In a DFB, the reactor consists of a combustor and a pyrolysis unit, with a heated sand bed serving as a heat carrier between these two components and operating in a circulating or bubbling fluidized regime. This configuration offers flexibility in terms of fine-tuning the reaction conditions towards the preferred product distributions. The integration of such a system with a petrochemical facility has been explored with biomass on the combustor side, with goal of recycling 100% of the carbon present in the plastic waste streams [6]. This system provides a promising alternative to fossil-free production of monomers for the chemical industry.

To characterize the species obtained from the process, usually a sample from the producer gas is taken acquired through a series of setups and the chemical species contained therein are quantified. Due to the large variety of chemical species contained in the gas, gas chromatography (GC) is conventionally used with different types of columns and detectors depending on the types of hydrocarbon molecules to be evaluated. The species concentrations are then reported in the literature in tables or presented in plain graphs of concentration vs. species, to indicate the respective yields under the particular process conditions.

While such presentation methods are straightforward, they have limitations. First, the results are limited to the species detected with the available characterization equipment setup. This may lead to an incomplete picture of the produced hydrocarbon groups, which is required for a comprehensive carbon balance. Second, the more conditions and feedstocks that are tested, the more challenging the data mining process becomes in order to understand the respective product distribution variations in cross-case studies. Third, the source of the variability is obscured, making it difficult to establish correlations between the graphed response and modified operational variables or to identify possible error sources in the dataset. Therefore, this thesis presents a model for data processing aiming to overcome these limitations. The model incorporates generic chemical characteristics and statistical considerations of the reaction system within a framework enclosed by hard constraints, such as elemental balances, topology of functions, and convergence criteria. In the global view, the model's construction enables the extraction of physically consistent information from the results obtained from steam cracking processes, thereby enhancing the predictive capabilities for non-measured carbon groups and improving the efficacy of data presentation for improved operational space explorations and data quality assessments.

In relation to the product distribution obtained from the steam cracking, the molecular composition of the feedstock plays a crucial role in determining the yields of specific species from the conversion process. The chemical conversion proceeds by primary free radical reactions that are initiated by the homolytic cleavage of the bonds in the polymer chain. These reactions break down the polymer chain, leading to the release of shorter chain structures into the local reaction environment. Subsequently,

secondary reactions take place, with these nascent volatiles in the local gas phase driving the formation of new chemical structures, such as aromatic rings and soot.

Overall, the temperature and the reaction medium limit the extent of the primary and secondary reactions. Nonetheless, the nature of the chemical bonds determines the types of radicals that are generated during the breakdown; consequently, it has a direct impact on the species obtained from the conversion process.

The likelihood that a free radical cleavage will occur is determined by the bond dissociation energy [8,9]. In general, primary reactions tend to break the chain at locations with low bond dissociation energy caused by anomalies in the electron density. Thus, the more homogeneous the bond dissociation energy is along the chain, the more random is the occurrence of the cleavage process. However, the presence of functional groups, such as aromatics, unsaturated bonds or heteroatoms, distorts the electron density distribution along the chain, creating sites that are susceptible to cleavage. Therefore, it is important to consider the feedstock's chemical structure when evaluating a particular product species distribution.

From a modeling perspective, predicting the ways in which various radical reactions and species will interact due to the inevitable interplay of primary and secondary reactions in a mixture of plastics presents a major challenge. Addressing this issue requires a comprehensive understanding of how the incoming composition influences the product distribution. The challenge becomes even more complex when dealing with heterogeneous feedstocks, which closely resemble real plastic waste streams.

Using data analysis techniques with real data from the steam cracking of highly heterogeneous mixtures can provide valuable insights into addressing the challenge mentioned above. By examining the input polymer blend and the primary products generated under specific thermodynamic conditions, it is possible to establish correlations that shed light on how the different carbon bonds in the polymer blend undergo reactions and transformations during the conversion process. This knowledge is essential for assessing the potentials for monomer and chemical recovery from various plastics and mixtures. Moreover, it paves the way for the development of a predictive model for the conversion behaviors of heterogeneous carbon-based materials, thereby enabling the evaluation of recycling routes and potential value chains. To illustrate this approach, this thesis summarizes the work performed with a pool of data from steam cracking experiments conducted on a semi-industrial scale 2–4-MW cracker within a DFB plant using heterogeneous, polymer-rich waste mixtures. The objective was to identify qualitative correlations between the polymeric composition of the feedstock and the resulting product distribution after cracking. A novel approach based on a carbon-based molecular classification of products and feedstock was introduced to create a generalization framework for studying these correlations.

In general, this thesis presents research endeavors that contribute to the development of mathematical tools aimed at enhancing the handling and analysis of the species distribution data obtained from the thermal cracking conversion of carbon-based feedstocks. By considering key chemical characteristics of the reaction system, the tools provide means for data quality assessments and quick estimation of valuable chemicals recovery potential from the steam cracking of plastic mixtures. The research provides insights into the relationship between product distribution and feedstock from a data analysis perspective, with the goal of creating correlation models that can be used in the operation and control of steam cracking DFB plants.

1.1. Aim and Scope

The general aim of this work is to develop a validated data analysis model that allows to improve the knowledge on the outcomes of the steam pyrolysis process and set a framework of data generalization that helps to unravel correlations between product species distribution and feedstock composition of polymeric mixtures.

To achieve this overarching goal, two specific research questions are addressed:

- I. How can the product species distribution and the chemical and mathematical constraints of a steam cracking system be linked together to improve the data quality and get physically and statistically meaningful observations from the reaction system with a model that can be experimentally validated?
- II. How to unravel correlations between the polymeric composition of a plastic mixture feedstock and its product species distribution from a steam cracking process by the creation of a common data framework established upon a carbon bond-based classification?

1.2. Publication's Contribution

This thesis comprises the main developments and findings from a set of three scientific papers. The research exploration has been conducted at both the theoretical and experimental levels. This document presents the equations and mathematical foundations of the developed models, as well as their validation using real industrial-scale data. In **Paper I**, the concept, mathematical background and experimental validation of a custom-made model, called the Parametric System Model (PSM), used for the data quality assessment is presented. **Paper II** focuses on understanding how the product distribution is influenced by the feedstock polymeric composition when cracking highly heterogeneous mixtures in a DFB. It presents a novel carbon classification framework that was developed to explore correlations between the products and the feedstock chemical structures. **Paper III** showcases experimental methods and characterization setups developed to get a quick and comprehensive carbon balance from the cracking gas product, with particular focus on GC with Vacuum Ultraviolet Spectroscopy (GC-VUV) as the characterization method.

2. Parametric system model development for data quality analysis

2.1. Model Formulation and Description

In any pyrolysis-based conversion process, the characterization outcomes are subject to three main sources of variation: changes to the feedstock; alterations to the operational thermodynamics; and measurement-related errors introduced by the experimental setup. Therefore, a model that is capable of correlating such sources with the acquired data must be inherently linked to the chemical nature of the process itself.

In line with this premise, the approach involves the processing of data obtained from steam cracking conversion using a mathematical transformation referred to as the Parametric System Model (PSM). The defining characteristic of this model is its integration within a framework governed by specific chemical and statistical characteristics of the chemical conversion process. The transformation encompasses a set of mathematical functions with distinctive topologies that introduce additional constraints to the framework (see Figure 1). This results in the creation of a highly constrained mathematical system that is tightly fitted to the physical nature of the conversion process. In the global view, such a physics-informed characteristic of the model provides physically consistent outcomes with several possibilities, such as those for: identifying inconsistencies in the measured data; estimating unmeasured quantities or species that may be inaccessible due to equipment limitations; and ranking certain measurements according to their relevance for the model's transformation, so as to minimize the sampling characterization effort.

In **Paper I**, the focus is on the application of the model for prediction of unmeasured species and data quality assessment of the data coming from steam cracking of a polyolefinic feedstock (polyethylene). The concept of creating a physics-informed framework that is based on mathematical functions constraining the data can also be applied to other types of feedstocks and mixtures.

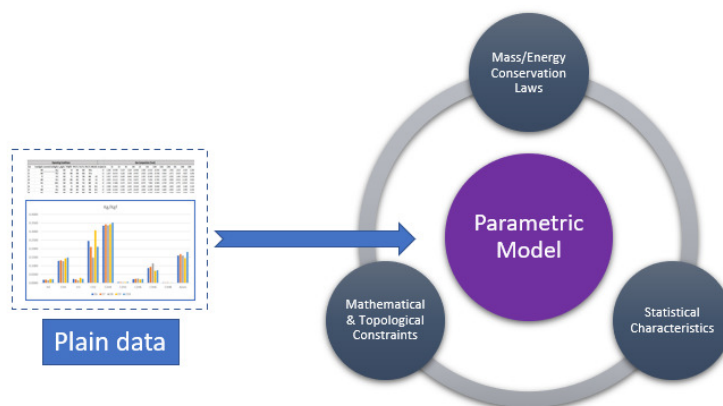


Figure 1. Conceptual schema for the "plain data" transformation into the proposed parametric model.

In the model formulation, the species contained in the product mixture are categorized into distinct groups: paraffins, olefins, aromatics, syngas and char, and treated as molecular systems. The model's core constraints are defined based on the system's conservation laws. In **Paper I**, only mass conservation is taken into account, expressed in terms of elemental balances. For a feedstock that is composed of carbon (C), hydrogen (H), and oxygen (O), the balances are mathematically defined using molar fractions, as presented in Equations (1)–(4).

$$n_{C,tot}^{pf} \sum_{k=1}^{\infty} X_{C,k}^{pf} + n_{C,tot}^{of} \sum_{k=1}^{\infty} X_{C,k}^{of} + n_C^{arom} + n_C^{CO} + n_C^{CO_2} + n_C^{char,out} = n_C^{fuel} + n_C^{char,in} \quad (1)$$

$$n_{C,tot}^{pf} \sum_{k=1}^{\infty} X_{C,k}^{pf} \gamma_k^{pf} + n_{C,tot}^{of} \sum_{k=1}^{\infty} X_{C,k}^{of} \gamma_{k,eff}^{of} + n_H^{arom} + n_H^{H_2,out} + n_H^{H_2O,out} = n_H^{fuel} + n_H^{H_2O,in} + n_H^{H_2,in} \quad (2)$$

$$n_O^{CO} + n_O^{CO_2} + n_O^{HC,out} + n_O^{H_2O,out} + n_O^{O_2,out} = n_O^{fuel} + n_O^{H_2O,in} + n_O^{O_2,in} \quad (3)$$

$$\gamma_k^{pf} = \left(2 + \frac{2}{k}\right); \quad \gamma_{k,eff}^{of} = \sum_{g=0}^{2\lfloor k/2 \rfloor - 1} X_{C,k,g}^{of} \left(2 - \frac{2g}{k}\right) \quad (4)$$

Here, n_a^s and $X_{a,k}^s$ correspond, respectively, to the number of moles and the molar fraction of the element $a \in \{C, H, O\}$ and the system $s \in \{pf, of, arom\}$, with *pf*, *of* and *arom* indicating the paraffin, olefin and aromatic groups, respectively. The subindex k represents the number of carbons in the paraffin or olefin chain, referred to here as the carbon group (shortened to: the k -group), and *tot* indicates the total amount. In Equation (2), γ_k^{pf} refers to the molar hydrogen to carbon (H/C) ratio for the paraffin system as a function of k . In addition, $\gamma_{k,eff}^{of}$ corresponds to the molar H/C that is effective for the olefins at a particular k , defined as the weighted molar fraction sum of the H/C ratios for all possible olefin species present in a particular k -group. The term g corresponds to the olefin species group, of a particular k , defined as having $2(k - g)$ hydrogens. In other words, g indicates the number of hydrogen pairs that are missing from the mono-ene case ($g = 0$). In Equation (3), $n_O^{HC,out}$ corresponds to the moles of oxygen in the produced hydrocarbon species that have oxygen atoms in their structures (for instance, some oxygenated aromatic species). The term $n_C^{char,in}$ accounts for external sources of char entering the system, for instance, char transported from the combustor side during the DFB cycle.

As demonstrated in Equations (1) and (2), paraffin and olefin species are classified according to their carbon groups. This classification requires a carbon number distribution representation, which is commonly used in the petrochemical industry to compare yields of specific species sizes and to assess the quality of products to be used as liquid fuels [10,11]. In the specific context of the study, such representation allows the modeling of group yields as mathematical sequences, which can be summed across an infinite range of k -groups. As explained in **Paper I**, relative to the hundreds of thousands of monomer units present in a real polymeric feedstock, limiting to the infinite in the series is essentially a mathematical formality to avoid restrictions imposed on the lengths of the species that can be formed in the cracking process. However, these series must be convergent, which imposes mathematical constraints on the sequence behavior or the functions associated with them.

Given the characteristics of the sequences, the molar fractions $X_{a,k}^s$, as defined in Equations (1) and (2), can be regarded as discrete probability functions for the evaluated molecular system, each of which is characterized by a finite set of parameters. This corresponds with the model's key mathematical transformation. Consequently, the paraffin and olefin sequences can be mathematically expressed as:

$$X_{C,k}^{pf} = f_{C,k}^{pf}(\alpha_1^{pf}, \alpha_2^{pf}, \dots, \alpha_n^{pf}); \quad X_{C,k}^{of} = f_{C,k}^{of}(\alpha_1^{of}, \alpha_2^{of}, \dots, \alpha_n^{of}) \quad (5)$$

$$X_{H,k}^{pf} = X_{C,k}^{pf} \gamma_k^{pf} = \gamma_k^{pf} f_{C,k}^{pf}(\alpha_1^{pf}, \alpha_2^{pf}, \dots, \alpha_n^{pf}); \quad X_{H,k}^{of} = X_{C,k}^{of} \gamma_{k,eff}^{of} = f_{H,k}^{of}(\beta_1^{of}, \beta_2^{of}, \dots, \beta_m^{of}) \quad (6)$$

$$n_{C,tot}^{pf} = \frac{\sum_{k=1}^{K_{ms}^{pf}} n_{C,k}^{pf,ms}}{\sum_{k=1}^{K_{ms}^{pf}} f_{C,k}^{pf}}; \quad n_{C,tot}^{of} = \frac{\sum_{k=2}^{K_{ms}^{of}} n_{C,k}^{of,ms}}{\sum_{k=2}^{K_{ms}^{of}} f_{C,k}^{of}} \quad (7)$$

Here, K_{ms}^{pf} and K_{ms}^{of} correspond to the maximum measured k -group for the paraffin and olefin species, respectively. The term $f_{a,k}^S$ is a discrete function with a semi-infinite support $k \in \{1,2,3 \dots\}$, which is defined with a finite set of shape parameters $\{\alpha_1, \dots, \alpha_n\}^S$ or $\{\beta_1, \dots, \beta_m\}$; $a \in \{C, H\}$ and $s \in \{pf, of\}$.

The main advantage of this approach is that it provides a closed-form solution to the equation system formed by Equations (1) and (2), while at the same time it can deliver the necessary topology and convergence criteria needed to satisfy the model's mathematical constraints.

2.2. Model Implementation and Additional Constraints

Following the parametric transformation of the paraffin and olefin sequences, the objective is to define a function f_k that can fit to the measured data using the minimum number of shape parameters, while acting as a solution to the system of equations. In this way, any estimations given by the function's mapping will comply with the mass conservation law.

In general, the function's formulation must satisfy the following conditions: 1) it must exhibit a decaying behavior with the possibility to become a monomodal and positively skewed function; 2) it must be sufficiently flexible to handle relatively large changes in species concentration, while remaining convergent and aligned with the measured data; 3) it needs to be defined with the fewest possible parameters; and 4) the function's form and predicted area must adhere to the conservation laws.

The first condition is based on the characteristic decaying behavior arising from the bond cleavage suffered by the homogeneous polyolefin chains as soon as they enter the hot reactor medium. The pyrolytic reaction progresses as the resulting molecules try to adopt more-stable structures and lengths. As a rule of thumb, the shorter the chain, the more stable it becomes.

In principle, the hotter the reaction medium, the more random and thorough the breakdown process becomes, since more energy is available to produce the scissions. At this point, the decomposition process can be seen as a stochastic system that is governed by events that can be described by a probability distribution function.

In its simplest form, the set of events in the chemical system can then be conceptualized as a system that comprises two types of elements: broken and unbroken bonds. If N_0 is the number of initial bonds, the probability q of finding a bond in the chemical system is defined by $q = N_b/N_0$, with N_b being the number of remaining bonds at time t . Then, the probability to find a broken bond is $p = 1 - q$ (as this can also be taken as the probability of breaking a bond at time t , it is a parameter that is directly related to the temperature). The probability of finding n consecutive unbroken bonds in n number of blinded pickups in the system is defined by q^n . A chain molecule of k carbons consists of a set of $k - 1$ unbroken bonds and 2 broken bonds at its extremes. Therefore, the probability of finding such a set of elements in the system will be $p^2 q^{k-1}$. From the carbon's perspective, the probability of finding a particular carbon in such a set will be $P_k = kp^2 q^{k-1} = kp^2(1 - p)^{k-1}$. This is commonly known as the Flory-Schultz distribution; it describes the probability of obtaining a chain of length k after the occurrence of random and identically independent scission events with probability p . It should be noted that this is a special case of the Negative Binomial Distribution for $k - 1$ successes and exactly 2 failures (see Figure 2).

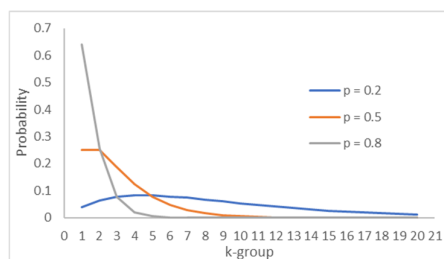


Figure 2. Flory-Schultz distribution.

This simple conceptualization illustrates the increasing abundance of shorter chains as the probability of a breaking event increases. Although the real-life case may be more complex, this simplified view offers a clear picture of the stochastic process that leads to the results obtained.

The second and third criteria aim for a robust model that is capable of fitting diverse process conditions while compressing the data without overfitting for an effective representation. This facilitates correlative and predictive analyses. The fourth criterion incorporates the restriction that the conservation laws impose on the conversion process (in the studied case, only mass conservation is considered).

As an example of an application, let's consider a high-temperature decomposition scenario that follows a Flory-Schultz distribution with high probability, as depicted for $p=0.7$ in Figure 2. Furthermore, assume that the experimental setup provides information only for the quantities of the first three aliphatic carbon group species. In the absence of prior information regarding the system's decomposition, the decreases in the quantities of the measured species serve as the initial indicator of the system's behavior.

Considering the mass conservation law, approximately 90% of the normalized mass in the distribution will be accounted for on the measured side. This significantly limits the range of possibilities for the $k \geq 4$ estimations. Given the probabilistic nature of the system for the domain of random breaking-down events, the topology must align with the behavior of the measured data and the restrictions imposed by the conservation laws, while ensuring convergence of the series in the limit to the infinity. At this point, the system becomes highly constrained. In that sense, the idea of assigning a solution function with an excessively large, insufficient, or non-convergent area to the unknown side should be discarded (see Figure 3). Alternatively, if the measured area is excessively long or short, thereby hindering the possibility for a convergent fit consistent with the observed trend, this suggests a need to review the outcomes of the experimental setup and check for potential data quality issues.

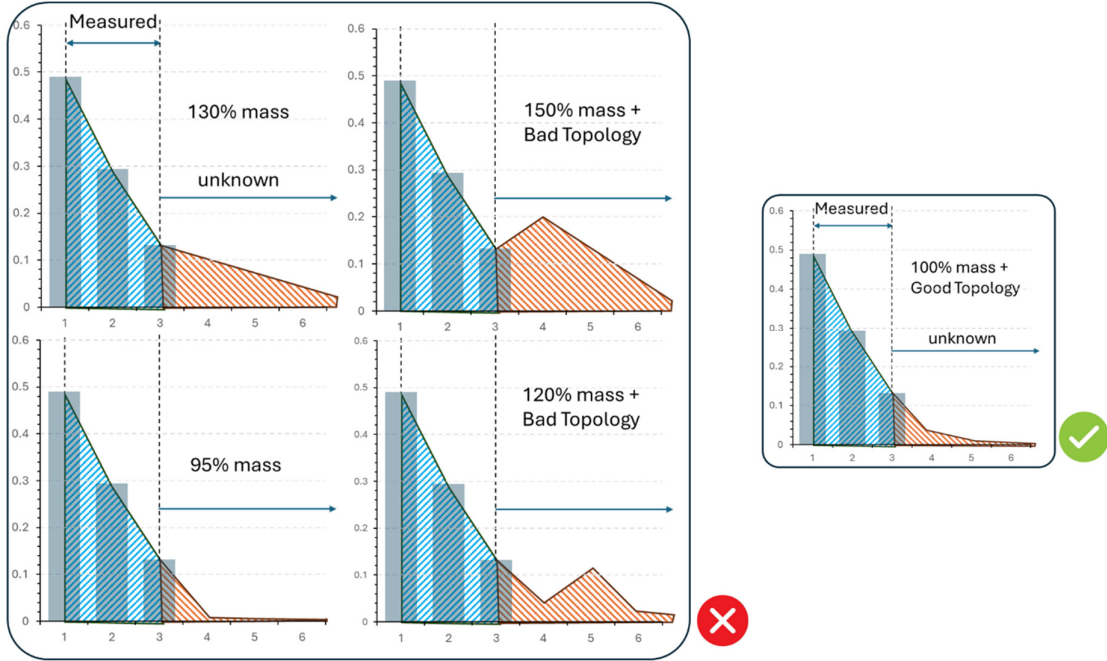


Figure 3. Examples of correct and incorrect cases of function fitting.

The realm of discrete distribution functions can provide the candidates that best fulfill all of the aforementioned conditions. Well-known discrete functions (such as Negative Binomial and Poisson) and discretized versions of continuous distribution functions were considered. Table 1 presents the various probability distribution functions evaluated in this study. It is noteworthy that given that the continuous functions family is larger than the discrete functions family, most of the bi-parametric functions utilized in the research arose from discretizing well-known continuous probability distributions [12].

Table 1. List of mono-parametric and bi-parametric distribution functions used in **Paper I**. The asterisk-marked rows correspond to heavy-tailed distributions. (Weibull is heavy-tailed for $0 \leq \beta \leq 1$).

Distribution's Name	Mathematical Expression
Geometric	$f_k(\alpha) = \alpha(1 - \alpha)^{k-1}; \quad 0 < \alpha < 1$
Flory-Schultz	$f_k(\alpha) = \alpha^2 k(1 - \alpha)^{k-1}; \quad 0 < \alpha < 1$
Poisson	$f_k(\alpha) = \alpha^{k-1} e^{-\alpha} / (k-1)!; \quad \alpha > 0$
Negative Binomial	$f_k(\alpha, \beta) = \Gamma(k + \beta - 1) \alpha^\beta (1 - \alpha)^{k-1} / (\Gamma(k) \Gamma(\beta)); \quad \beta > 0, \alpha \in [0, 1]$
Conway-Maxwell	$f_k(\alpha, \beta) = \alpha^{(k-1)} / (Z(\alpha, \beta) * ((k-1)!)^\beta); \quad \alpha, \beta > 0$
Burr *	$f_k(\alpha, \beta) = (1 + (k-1)\alpha)^{-\beta} - (1 + k\alpha)^{-\beta}; \quad \alpha, \beta > 0$
Fréchet *	$f_k(\alpha, \beta) = e^{-(k/\alpha)^{-\beta}} - e^{-((k-1)/\alpha)^{-\beta}}; \quad \alpha, \beta > 0$
Dagum *	$f_k(\alpha, \beta) = (1 + k^{-\alpha})^{-\beta} - (1 + (k-1)^{-\alpha})^{-\beta}; \quad \alpha, \beta > 0$
Gompertz	$f_k(\alpha, \beta) = e^{-\alpha(e^{\beta(k-1)} - 1)} - e^{-\alpha(e^{\beta k} - 1)}; \quad \alpha, \beta > 0$
Weibull *	$f_k(\alpha, \beta) = e^{-((k-1)/\alpha)^\beta} - e^{-(k/\alpha)^\beta}; \quad \alpha, \beta > 0$
Gamma	$f_k(\alpha, \beta) = \gamma(\alpha, \beta(k-1)) / \Gamma(\alpha) - \gamma(\alpha, \beta k) / \Gamma(\alpha); \quad \alpha, \beta > 0$
Lomax *	$f_k(\alpha, \beta) = (1 + (k-1)/\alpha)^{-\beta} - (1 + k/\alpha)^{-\beta}; \quad \alpha, \beta > 0$
Gamma Inverted *	$f_k(\alpha, \beta) = \gamma(\alpha, \beta/(k-1)) / \Gamma(\alpha) - \gamma(\alpha, \beta/k) / \Gamma(\alpha); \quad \alpha, \beta > 0$

In general, the flexibility level of a function increases with the number of parameters that it incorporates. In particular, the family of bi-parametric functions has proven highly adaptable for describing diverse physical phenomena encountered across various fields. Among these functions,

heavy-tailed distributions (indicated with asterisks in Table 1) exhibit remarkable robustness in terms of capturing significant variations within a dataset, particularly when dealing with a substantial number of outliers. This flexibility arises from their characteristic tails, which decay at a slower rate than functions with exponential decay, and this makes them well-suited for modeling extreme events, such as the ones found in natural phenomena, e.g., survival times, river discharges, etc. [13].

In essence, the fundamental approach involves utilizing the measured data as reference points, the experimental uncertainties as constraints, and Equations (1) and (2) to obtain a new set of equations with the aim of determining the specific shape parameters $\{\alpha_i\}$ for a given function. If a finite and real set of parameters $\{a_i\}$ can be identified, the corresponding function becomes a solution to the PSM's equation system. For a certain number of parameters n and m , the minimum number of observables is $n+1$ and $m+1$, respectively. Thus, the experimental setup must adapt to such data requirements.

The unique nature of most distribution functions requires the application of non-linear solvers or Monte Carlo methods to find the parameter set that fulfills all the conditions imposed by the equation system. Once the shape parameters are determined, the function can be visualized by overlaying it onto a column bar graph representing species in *mol/kgf* versus the respective k -groups.

For the hydrogen function case, an additional constraint can be formulated which describes the behavior of the H/C ratio of the olefins system, i.e., the term $\gamma_{k,eff}^{of}$ presented in Equation (4). For each k , this quantity varies between 2 and the lowest possible H/C ratio determined by the chain length and carbon valency at $g = 2[k/2] - 2$. Therefore, the olefin's hydrogen function is confined within a specific region. The upper limit is set by the mono-ene case function given by Equation (8), while the lower limit corresponds to the fully unsaturated scenario expressed in Equation (9), when every possible hydrogen has been extracted from the k -group chain. An intermediate case is defined as the fully conjugated state, defined by Equation (10), when the chain only contains intercalated double bonds. The olefin's hydrogen function must fall within this defined range to fulfill the chemical characteristics of the molecular system.

$$f_H^{high} = 2n_{C,k}^{of} \quad (8)$$

$$f_H^{low} = \frac{1}{k} ((2k + 2) - 4[k/2])n_{C,k}^{of} \quad (9)$$

$$f_H^{mid} = \frac{1}{k} ((2k + 2) - 2[k/2])n_{C,k}^{of} \quad (10)$$

2.3. Validation Method

The oxygen balance was used as an additional equation to calculate a relevant process quantity in a DFB system, known as the Bed's Oxygen Transport (BOT), and to feature the data quality assessment potential of the model to the experimental results.

In DFB reactors, the BOT phenomenon occurs when the bed material contains oxygen-carrying species. The circulating bed serves as a carrier medium, transferring heat from the combustor to the cracker chamber and transporting char and active species between the cracker and combustor. Even seemingly inert bed materials, such as silica sand, may contain traces of transition metal oxides, such as Fe_2O_3 , which act as oxygen donors. These elements influence the cracking process and can alter the gas product composition to some extent. Furthermore, ashes carried by the bed from the combustor side can serve as significant sources of oxygen. Elements such as calcium participate in redox cycles [14]

form compounds such as CaSO_4 under oxidizing conditions within the combustor and this is transformed into CaS in the reductive environment of the cracker.

The hydrogen and oxygen balances are essential to calculate the BOT based on product composition. By rearranging the oxygen balance in Equation (3) and applying the water H/O molar ratio of 2, the BOT can be derived as in Equation (11):

$$\begin{aligned} n_O^{CO} + n_O^{CO_2} + n_O^{HC,out} - (n_O^{H_2O,in} - n_O^{H_2O,out}) &= n_O^{fuel} + n_O^{O_2,in} - n_O^{O_2,out} \\ \Rightarrow \Delta n_O^{O_{ext}} = n_O^{O_2,in} - n_O^{O_2,out} &= n_O^{CO} + n_O^{CO_2} + n_O^{HC,out} - \frac{1}{2} \Delta n_H^{H_2O} - n_O^{fuel} - n_O^{leak} \end{aligned} \quad (11)$$

Now, from the hydrogen balance, the level of water conversion ($\Delta n_H^{H_2O} = n_H^{H_2O,in} - n_H^{H_2O,out}$) can be estimated as:

$$\Delta n_H^{H_2O} = \left(n_{C,tot}^{pf} \sum_{k=1}^{\infty} X_{C,k}^{pf} \gamma_k^{pf} + n_{C,tot}^{of} \sum_{k=1}^{\infty} X_{C,k}^{of} \gamma_{k,eff}^{of} + n_{H,total}^{arom} + n_H^{H_2,out} \right) - (n_H^{fuel} + n_H^{H_2,in}) \quad (12)$$

The term $\Delta n_O^{O_{ext}}$ in Equation (11) refers to the variation of oxygen entering or leaving the reaction environment due to external sources other than the fuel or fluidization steam. Positive values indicate that the reaction consumed external oxygen, while negative values imply oxygen removal by an external agent. In the absence of a deliberate oxygen input flow, two external oxygen sources can be identified: unintended air leakage into the cracker (n_O^{leak}), and the circulating bed material. Typically, leakage is minimal thanks to periodic maintenance of the reactor. However, for non-nitrogenous fuels, air leakage can be quickly calculated through the nitrogen balance with the detected level of N_2 and the air O/N ratio. Then, Equation (11) defines the oxygen transported into the system by the bed, i.e., the BOT.

Under typical DFB conditions, Equation (11) essentially links the oxygen transported by the bed during fuel conversion with the hydrogen balance. This means that the parametric functions for hydrogen assigned to the paraffin and olefin systems, as shown in Equation (6), contain key information regarding the species distribution to be used in the estimation of the BOT in the reaction system.

To validate the PSM estimations, an experimental approach utilizing a High-Temperature Reactor (HTR) [15] in a parallel sampling stream was implemented (see Figure 8). In this method, gas products react further with steam at very high temperatures in the HTR ($\sim 1,700^\circ\text{C}$), generating only syngas. The BOT can also be calculated using the outcomes of the HTR in Equation (11), albeit in a simplified form due to the complete reforming of the carbon species in the product gas to produce H_2 , as presented in Equation (13).

$$\Rightarrow \Delta n_O^{O_{ext}} \Big|_{HTR} = n_O^{CO} + n_O^{CO_2} - \frac{1}{2} \left(n_H^{H_2,out} - (n_H^{fuel} + n_H^{H_2,in}) \right) - n_O^{fuel} - n_O^{leak} \quad (13)$$

Since both calculations stem from the same sampled gas batch, the result from Equation (13) should align with that calculated using Equation (11), serving as validation of the PSM estimations.

3. Unraveling Correlations between the Steam Pyrolysis Product Distribution and Polymer Composition

The molecular composition of a polymeric feedstock plays a crucial role in the definition of the final cracking product distribution. As seen before, in thermal cracking, the primary objective is to break macromolecules into smaller structures, while retaining key elements of their composition. This involves subjecting polymers to high heating rates and temperatures, thereby promoting primary reactions that are characterized by bond breakage and free radical mechanisms. Subsequent secondary reactions occur in the emergent local gas phase, leading to the transformation of volatiles into intricate structures such as polyaromatics and, ultimately, soot [16,17]. In particular, in a steam-rich environment, these volatile compounds are further transformed via reforming reactions into syngas ($H_2 + CO$). Figure 4 shows a schematic representation of this decomposition process.

The specific structure of a polymer is central to determining its susceptibility to free radical bond-breaking reactions. The formation of radicals through homolytic degradation in a high-temperature process is strictly linked with the bond dissociation energy, a scalar that is affected by the polymer chemical structure [16,18]. The presence of reactive sites, which increase the likelihood of radical cleavage, is often due to atomic charge heterogeneities within the molecular chain structure [8,9]. Such heterogeneities are typically induced by the presence of functional groups, such as alkyl, carbonyl and nitrile groups, as well as halogens and aromatic rings. These groups can act as radical initiators or participate in the secondary reactions that generate a diverse array of product species. Understanding these factors in the decomposition of polymer structures is pivotal to identifying correlations between the products and feedstock in the cracking process.

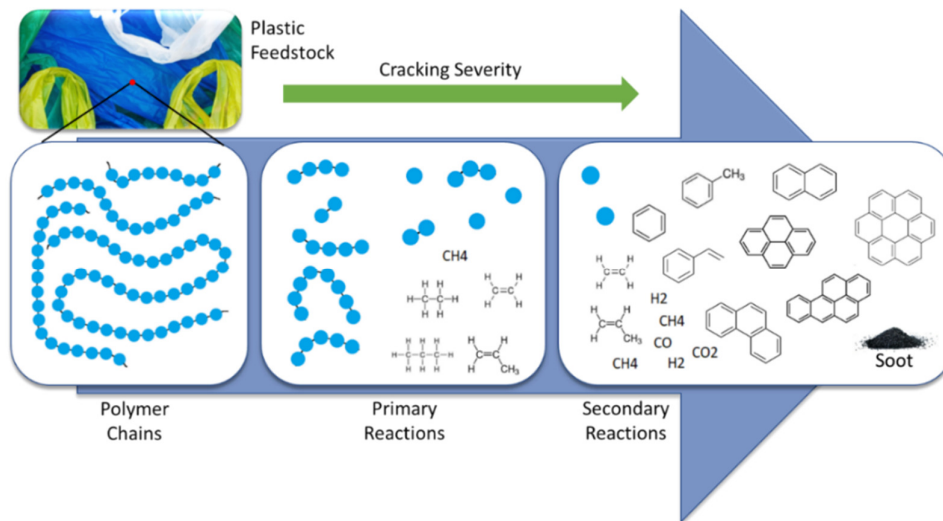


Figure 4. Polymer chain decomposition through primary and secondary reactions during the cracking process.

Polymer Categories

The polymers found in plastic waste can be categorized into three groups: aliphatic polymers, aromatic-containing polymers, and heteroatom-containing polymers, with each group exhibiting distinct behaviors during pyrolysis. Aliphatic polymers, such as polyethylene (PE) and polypropylene (PP), undergo random scission at low temperatures ($>400^\circ C$), producing diverse molecule lengths. At

higher temperatures (e.g., 700°–800°C), end-chain scission occurs, yielding shorter molecules such as methane, as well as aromatics and polyaromatics due to the secondary reactions [19,20]. In the category of aromatic-containing polymers, compounds such as polystyrene (PS) and polyethylene terephthalate (PET) yield aromatic rings directly from their existing structures. For instance, PS can recover up to 75% of its styrene at a relatively low temperature (450°C) and can attain 78.7% recovery at 600°C [21].

Heteroatom-containing polymers, including oxygen, chlorine, fluorine, and nitrogen, exhibit diverse thermal decomposition paths that lead to recombination reactions or the formation of stable molecules such as CO/CO₂, HCl, and NH₃. Nitrogen-containing polymers such as PU and PA undergo rearrangements at temperatures in the range of 250°–450°C, producing linear fragments with functional groups such as -amino (-CH₂-NH₂) and -nitrile (-CN) groups, concomitant with the elimination of CO₂ and H₂O [22,23]. Chloride-containing polymers such as PVC undergo significant aromatization post-dehydrochlorination due to the weakening of the bond energy by the chlorine's electronegativity. This forms reactive sites that can react with other radicals or create double bonds that lead to the formation of aromatic or polyaromatic structures [24–26].

In waste streams, the most-common polymers, e.g., polyolefins, decompose almost fully into gas at temperatures in the range of 500°–600°C [20]. Temperatures outside this range cause further degradation of the gas phase, breaking long chains into simpler monomeric structures [C₂–C₄ and benzene, toluene, xylene, and styrene (BTXS)], which are valuable for chemical recycling. Polyolefins experience this phenomenon at temperatures in the range of 600°–900°C, although higher temperatures risk reducing the monomer yield, and may cause unwanted secondary cyclization reactions that result in polyaromatic structures [20,27,28]. The study described in **Paper II** was conducted at 800°C to balance monomer recovery with the control of harmful emissions related to heteroatoms (in the form of dioxins) [29,30]. The focus of the study was on the hydrocarbon fraction and carbon conversion slate of the cracking products.

3.1. Polymeric composition estimation method for unknown plastic mixtures

In typical plastic waste streams, the polymeric composition is often unknown. These streams contain a diverse mix of plastics, including polyethylene (PE), polypropylene (PP), polyvinyl chloride (PVC), and polyethylene terephthalate (PET), among others. Manual sorting can give estimations of the polymeric slate, albeit with an unavoidably large uncertainty and substantial effort, making it impractical for continuous waste streams flows. These materials, even when sorted, remain heterogeneous due to functionalization, dyeing, and other modifications that are tailored for specific functions. Metals and inorganic compounds are also present in waste streams due to the preceding sorting and handling processes.

Strategies for online estimation of the polymeric composition include direct characterization methods, including x-ray diffraction and spectroscopic analyses with NIR or FT-IR [31,32]. Yet, these methods may prove inadequate for highly heterogeneous mixtures and bulk streams, due to the presence of composites, fillers, different colored materials, and high ash contents. Preprocessing is often necessary, making the entire characterization procedure both time-consuming and resource-intensive. To overcome these limitations, numerical models emerge as valuable tools. These methods leverage mathematical algorithms and computational models to estimate the compositions of complex mixtures based on mass and energy conservation laws. The models offer a quicker and more-cost-effective way to obtain physically congruent approximations of the polymer composition, without requiring specialized and expensive equipment.

In **Paper II**, a numerical model was implemented building up a system of equations based on the elemental balances obtained from the ultimate analysis of the feedstock. Mass and energy conservation, in the form of the Low Heating Value (LHV), was also added to the system to increase the physical congruence of the model to the polymeric composition. In general, from the conservation laws, for a particular feedstock blend f , the total mass and LHV will be the sum of the contributions of all the polymeric compounds j present in the blend. Equations (14)–(16) condense this principle for expression in the Einstein notation form (E.N):

$$\sum_j x_j^f a_{ji}^f = a_i^f \Rightarrow a_j^{i,f} x^{j,f} = a^{i,f} \quad (E.N) \quad (14)$$

$$\mathbf{1}_j x^{j,f} = m_{tot}^f \quad (E.N) \quad (15)$$

$$LHV_j x^{j,f} = LHV^f \quad (E.N) \quad (16)$$

where a_j^i is the mass fraction matrix ($i \times j$) of the element $i \in \{C, H, O, N, Cl, \dots\}$ in polymer $j \in \{PE, PP, PVC, \dots\}$ (units: kg_i/kg_j), x^j is the mass fraction vector ($j \times 1$) of polymer j within the feedstock blend (units: kg_j/kg_f), and $a^{i,f}$ is the mass fraction vector ($i \times 1$) of element i in the feedstock (kg_i/kg_f). The term $\mathbf{1}_j$ represents a ($1 \times j$) covariant vector of ones, and m_{tot}^f is the sum of the mass fractions of the element set evaluated. All quantities are evaluated for a particular feedstock f .

The final system of equations corresponds to a typical linear system of the form $Ax = b$, as expressed in Equation (17). In the real system, the target output vector b will have an associated experimental uncertainty Δb derived from the ultimate analysis of the feedstock. Then, the equations are transformed into inequalities that span over that uncertainty, creating a constrained frame for the solution space. Equations (18) and (19) show the additional constraints imposed on the system.

$$A_j^n x^j = b^n; \quad A = \begin{bmatrix} a_j^i \\ LHV_j^f \\ \mathbf{1}_j \end{bmatrix}, b = \begin{bmatrix} a^{i,f} \\ LHV^f \\ m_{tot}^f \end{bmatrix} \quad (17)$$

$$0 \leq x^j \leq 1, \quad \forall j \quad (18)$$

$$|Ax - b| \leq \Delta b \quad (19)$$

The system of Equation (17) is not always consistent (number of independent columns of A is equal to the set j size) or precisely determined ($size\{j\} \neq size\{n\}$ where $\{n\}$ is the eq. set). For example, similar chemical formulas or more polymers in the blend than detected elements in the ultimate analysis can lead to problems for the matrix system to find a unique solution. To address this issue, mathematical optimization of a defined loss function constitutes a robust method to find the best estimates for solving the equation system.

In **Paper II**, convex optimization methods are explored. These methods aim to find optimal solutions to matrix problems when the loss function and the constraints are defined by convex functions, as is the case with the problem at hand. Typically, the loss function is defined in its general form as Equation (20). For the case in study, two different loss functions were tested and derived from the general form, and they are defined as the sum squared error (sme) and the fractional error (fe) of the matrix system. These are presented in Equations (21) and (22), and the constraints are those defined in Equations (14) and (15).

$$L(y) = y^T P y + c^T y + d \quad (20)$$

$$\text{smc: } y = Ax - b; P = \mathbf{I}, c = \mathbf{0}, d = 0 \Rightarrow L(x) = (Ax - b)_n (Ax - b)^n = \|Ax - b\|_2 \quad (21)$$

$$\text{fe: } y = |Ax - b|; P = \mathbf{0}, c^n = \frac{1}{b^n} \forall n, d = c_n b^n \Rightarrow L(x) = c^T |Ax - b| = |c_n A_j^n x^j - d| \quad (22)$$

where $\| \cdot \|_2$ is the Euclidean norm for a vector (or L2-norm).

Among the set of algorithms used to implement the convex optimization, first-order solvers, known as the Splitting Conic Solver (SCS) and Operator Splitting Quadratic Program (OSQP), were used due to their robustness and potential scalability to solve large systems [33,34]. These solvers were tested and implemented as a Python library under the Apache License using a domain-specific language (DSL) called CVXPY [35].

To avoid pre-defined or biased results, optimization over the equation system's hyperparameter set is needed. In this case, the set is comprised of the different polymer compounds, the chemical elements considered in the balance, the loss functions, and the solvers used. A grid searching method over all possible combinations of the hyperparameters (see Table 2) was implemented to identify the best-approximated set, using the total sum of the residuals of the elemental balances and the LHV as the optimization metric.

Table 2. Hyperparameter set used to perform the tuning process.

Condition	Possible Values
Polymers	PE, PP, PVC, Cell, PS, PAN, PET, PA, PU, ABS, Nrubber, TRubber, PMMA, PC
Elements	C, H, Cl, O, N, S
Loss Functions	Sum_Squares, Fractional_Err
Solvers	SCS, OSQP

The analyzed plastic blends in **Paper II** were assumed to be free of organic or inorganic additives, and any impurities were treated as inert ash. Only the pure polymer compounds most-commonly found in waste mixtures were considered for the calculation. The relevant chemical parameters for the polymers are presented in Figure 5.

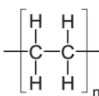
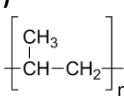
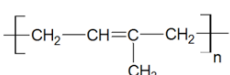
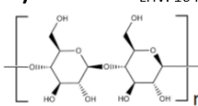
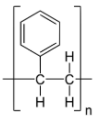
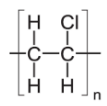
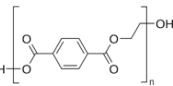
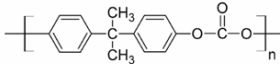
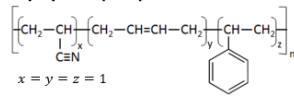
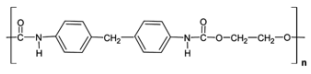
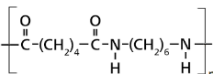
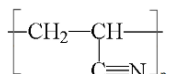
Polyethylene (PE)  MF: C_2H_2 MW: 28.05 g/mol LHV: 45 MJ/kg	Polypropylene (PP)  MF: $(C_3H_6)_n$ MW: 42.08 g/mol LHV: 45 MJ/kg	Polyisoprene (Rubber)  MF: $(C_5H_8)_n$ MW: 68.12 g/mol LHV: 43 MJ/kg
Cellulose (Cell)  MF: $(C_6H_{10}O_5)_n$ MW: 162.14 g/mol LHV: 16 MJ/kg	Polystyrene (PS)  MF: $(C_8H_8)_n$ MW: 104.15 g/mol LHV: 42 MJ/kg	Polyvinylchloride (PVC)  MF: $(C_2H_3Cl)_n$ MW: 62.50 g/mol LHV: 23 MJ/kg
Polyethylene-terephthalate (PET)  MF: $(C_{10}H_8O_4)_n$ MW: 192.17 g/mol LHV: 23 MJ/kg	Polycarbonate (PC)  MF: $(C_{16}H_{14}O_3)_n$ MW: 254.28 g/mol LHV: 31 MJ/kg	Acrylonitrile Butadiene Polystyrene (ABS)  MF: $(C_{15}H_{17}N)_n$ MW: 211.31 g/mol LHV: 40 MJ/kg $x = y = z = 1$
Polyurethane (PU)  MF: $(C_{17}H_{16}N_2O_4)_n$ MW: 312.32 g/mol LHV: 22 MJ/kg	Polyamide (PA)  MF: $(C_{12}H_{22}N_2O_2)_n$ MW: 226.32 g/mol LHV: 30 MJ/kg	Polyacrylonitrile (PAN)  MF: $(C_3H_3N)_n$ MW: 53.06 g/mol LHV: 31 MJ/kg

Figure 5. Polymers commonly found in waste streams. MF, molecular formula; MW, molecular weight; LHV, low-heating value.

Natural rubber (NRubber in Table 2) was considered as pure polyisoprene, and tire rubber (TRubber), was taken as 71% natural rubber and 29% carbon black as filler [36,37]. Polymethyl methacrylate (PMMA, $C_5H_8O_2$; MW, 100.1 g/mol; LHV, 24 MJ/kg) and wool, with parameters based on typical wool fiber [38], were also included in the analysis.

3.2. Carbon bond-based classification system model

As the diversity of polymers in a heterogeneous mixture converge into the cracker, the structural characteristics of each polymer type will come forth, shaping the resultant product distribution obtained from the cracking process. In order to explore the relationship between the polymer composition of the feedstock and the cracking product distribution at the data analysis level, a systematic classification framework for carbon molecules was developed. Cracking products were sorted into three fundamental categories: Cox species, aliphatics, and aromatics. Similarly, the polymers contained in the waste material were categorized based on a three-group system that reflected their carbon structures: 1) carbons in C-X bonds, where X represents heteroatoms such as O, Cl, N, etc.; 2) carbons in aliphatic bonds (C-AL), encompassing paraffinic and olefinic structures; and 3) carbons in aromatic bonds (C-AR), accounting specifically for aromatic rings. This classification strategy enables comparisons and cross-correlation analysis at the bond group level between the products and the feedstock. Based on this classification, the elemental mass fractions of the list of polymers presented in Figure 5, as well as the carbon molar fractions for each of the defined groups, are presented in Figure 6.

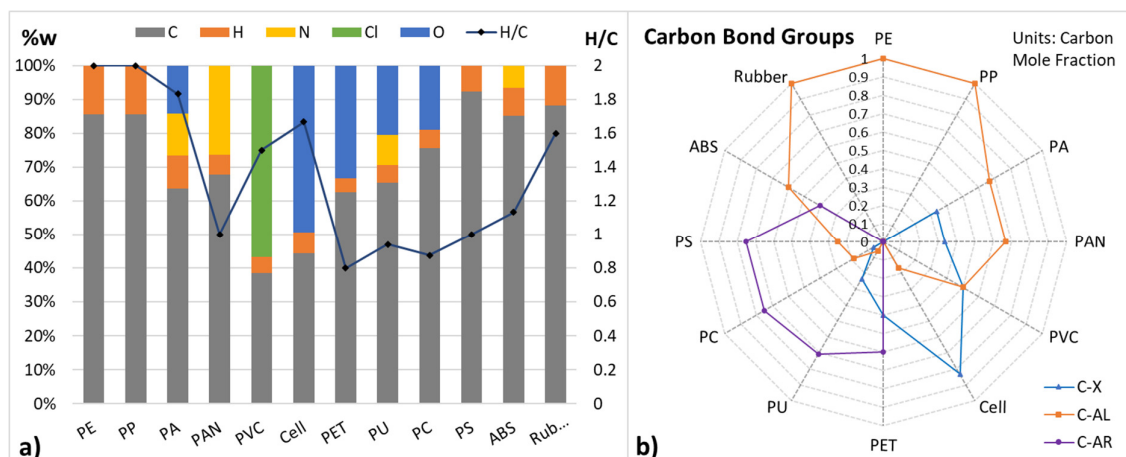


Figure 6. Chemical characteristics of the polymers commonly found in plastic waste streams. Panel a, Elemental compositions and H/C ratios. Panel b, Carbon mole fractions of the polymers according to the three defined bond groups (X refers to a heteroatom of O, N and Cl). AL, aliphatic; AR, aromatic.

The data depicted in Figure 6 highlight the chemical diversity of the evaluated polymers. Within a typical waste stream, a diverse arrangement of chemical structures appears, distinguished by different H/C ratios and different shares of the carbon-bond groups. Aliphatic polymers, such as PE and PP, exhibit higher H/C ratios, while PS and PET display low H/C ratios, characteristic of ring-based structures. In contrast, cellulose (cell) and PVC stand out due to their high heteroatom mass contents.

In a global perspective, The work performed in **Paper II** demonstrates the utility of the developed structure-informed framework as a common data analysis basis for elucidating qualitative relationships between heterogeneous feedstock compositions and their associated product distributions. Furthermore, the idea of evaluating the polymeric conversion through the transformation of representative carbon-bond groups can be expanded into a more-complex set, Which can increase the analysis resolution for cases in which the elemental and structural composition are similar. For instance, the addition of a methyl-bond group can allow to decoupling of certain polymers, such as PE and PP which share the same elemental composition.

Beyond the scope of **Paper II**, the results obtained from applying the framework to find correlations constitute a proof of concept that paves the way for quantitative analysis of the linkages between polymeric feedstocks and cracking products. This possibility may lead to the implementation of an additional constraint layer onto the system of equations presented in Equation (17). Similar to the possibility of obtaining an elemental analysis of C, H, O, N, S, Cl from the product gas using a combustor and a high-temperature reactor (see [15,39]), this constraint can also be derived from the process outputs. This feature makes it suitable for a continuous online estimation system. Details of the mathematical formulation of such a constraint can be found in Section 6, along with the bridge that can be established between the approaches presented in **Papers I** and **II** for the online estimation of polymeric compositions in heterogeneous mixtures.

4. Experimental Setup

All of the experiments were conducted at the Chalmers Power Central facility, where a DFB Gasifier/Cracker is coupled with a Circulating Fluidized Bed combustor that runs with biomass wood chips. Silica sand was used as the bed material and the reactor was fluidized with steam. The feedstock flows for the cracker processes are in the range of 40–160 kg/h of plastic materials, while the CFB is operated with flows in the range of 1,500–3,000kg/h of wood chips. A small flow of high-purity helium (35 Ln/min) is added along with the steam (~150 kg/h), to serve as a tracer gas for the species quantification. The DFB configuration allows the continuous removal of the produced char, along with the bed material, transporting it back to the combustor side. Following conversion of the feedstock, a sample stream is continuously extracted at the reactor's exit (~10 Ln/min) and the remaining product gas (~3,500 Ln/min) is conducted back to the combustor (see Figure 7).

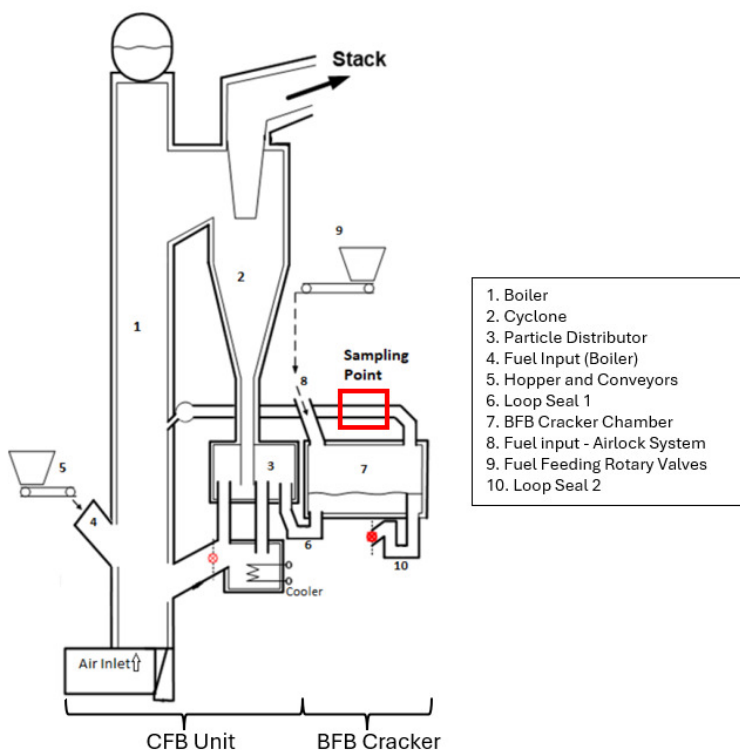


Figure 7. Schematic of the Chalmers power plant and gasifier (modified from [40]).

The sampled stream passes through a high-temperature (~350°C) particle filter and then splits into two parallel streams (see Figure 8). The first stream passes through an isopropanol quenching loop, to remove condensable species such as water, long hydrocarbon chains, and aromatics. Further cooling is performed in a chiller, to ensure that no species condense downstream. After conditioning, the gases are pumped into a Micro-Gas Chromatograph Varian CP4900 (GC1) equipped with a Thermal Conductivity Detector (TCD). The micro-GC has two channels and uses Molsieve 5Å (MS5Å) and PoraPLOT Q columns with argon and helium as carrier gases, respectively. Permanent gases and C1–C3 hydrocarbon species can be characterized online by sampling from the continuous gas stream at 3-minute intervals. A weekly calibration of the chromatograph is performed using five different concentrations of the expected species in the dried gas (H₂, He, N₂, O₂, CO, CO₂, CH₄, C₂H₂, C₂H₄, C₂H₆, C₃H₆ and C₃H₈).

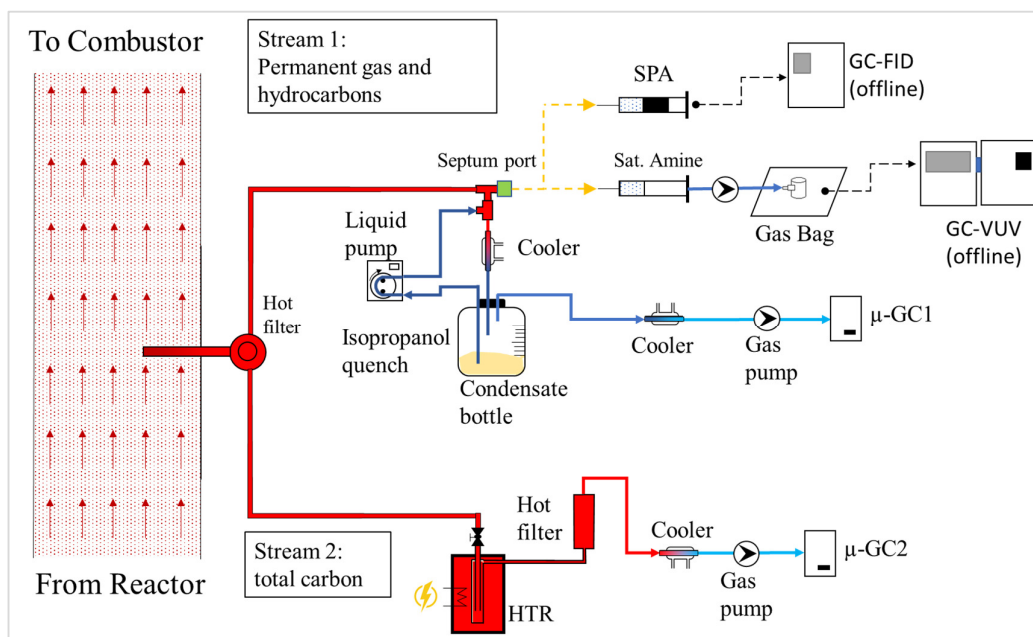


Figure 8. Sampling setup to characterize the permanent gases, hydrocarbons (aliphatics and aromatics) and total carbon in the reactor gas flow.

For **Papers I** and **III**, an additional sampling setup was used to characterize the C₄+ species in a GC-VUV. From a septum port located before the isopropanol loop, a gas sample is drawn through a saturated amine that acts as a filter for water and is collected into a gas bag at room temperature for characterization in the GC-VUV. For **Paper I**, the chromatograph is equipped with an Rxi-1-HT column (Fused silica: length, 60 m; ID, 0.250 mm; film thickness, 0.25 μm). To improve the characterization time and the resolution of peaks, in **Paper III**, the column used was the J&W CP-Sil 5 CB, CP7670 (Fused silica: length, 25 m; ID, 0.250 mm; film thickness, 1.2 μm). The carrier gas was hydrogen, and nitrogen was used in the detector to make the gas cell inert.

Regarding this last setup, the study presented in **Paper III** focuses on establishing a formal methodology for sampling and characterization based on GC-VUV. This methodology provides a comprehensive carbon balance for the cracking products slate within a reasonable timeframe, with the goal of future implementation for online characterization. The work showcases different methodologies, comparing the proposed sampling method with more-traditional methods in terms of analytic timeframe and level of species resolution. The evaluated methodology based on GC-VUV achieved optimal quantification for C₄–C₁₈ species in considerably less time than the more-conventional techniques, such as those based on solid phase adsorption described later.

From the same sampling port, a Solid Phase Adsorption (SPA) method is applied to obtain the aromatic fraction. In this method, the gas is subjected to suction with a 100 ml syringe at a constant rate, forcing it to pass through an adsorbent column (Supelclean ENVI-Carb/NH₂ SPE columns), which consists of an amine adsorbent layer (500 mg) followed by an activated carbon layer (500 mg). The adsorbed aromatics in the SPA column are subsequently eluted into a vial that contains a mixture of dichloromethane, isopropanol, and acetonitrile (8:1:1) using hexylbenzene and 4-ethoxyphenol as internal standards at concentrations suitable for the species quantification (~12,000 mg/L and ~250 mg/L, respectively). The vial is analyzed in a Bruker GC430 GC coupled with a Flame Ionization Detector (FID) and equipped with a mid-polar BR-17 MS (BR85877) column using H₂ as the carrier gas. Twenty-eight different aromatic species are quantified with boiling points ranging from monoaromatics, such

as BTXS, to polyaromatics, such as naphthalene, anthracene, and triphenylene. More details regarding this method and the measured species can be found elsewhere [41].

The second hot stream flows through a HTR that is electrically heated to $\sim 1,700^{\circ}\text{C}$ for the complete reforming of all hydrocarbon species by the steam contained in the raw gas. After leaving the reactor, the gases are filtered to remove soot and cooled down to remove excess water before being pumped into another micro-GC Varian CP4900 (GC2). The gases are expected to be almost 100% pure syngas (H_2 , CO and CO_2) containing the corresponding amount of helium, which allows one to estimate the total carbon in the producer gas and to derive an indirect estimation of the char yield. The efficacy of the reforming process is determined according to the amount of methane detected (close to zero). The HTR operates continuously and in parallel with the remainder of the described sampling process. After completing the measurement set, the HTR reactor is flushed with air to burn out any particles of soot that may have formed during the reforming process, and the corresponding carbon amount is measured in terms of the CO_2 produced.

4.1. Materials and Process Conditions

Pure PE (C: 85%; H: 15%) in the form of pellets was used as the feedstock for the studies conducted in **Paper I** and **Paper III**. For the case of **Paper II**, four representative material blends were used as feedstocks for the cracking process: Reject from Cardboard Recycling (CRB); Cable Plastics (CP); Textiles (TXT); and Automotive Shredder Residue (ASR). PE was also tested in **Paper II**, albeit as a reference material for comparison purposes. All four heterogeneous materials have in common that they are residues from post-consumer recycled products. The expected compositions of the materials and their ultimate analyses are shown in Table 3 and Table 4, respectively. For ASR, two different batches with different elemental compositions, resulting from different rejection processes, were analyzed. The “Polymer Types” column in Table 3 represents the different plastics that are expected to be present in the material given the source of the rejected stream, although their shares are unknown. The polymers classified as “Others” are taken as optional in the numerical estimation.

Table 3. Heterogeneous materials used in **Paper II** with their respective polymer compositions and general characteristics.

Material	Polymer Types	Chemical Characteristics	Description
Cardboard Recycling (CBR)	PE/PP, PET, Cellulose, PVC (Others: PU, PA, PS)	- High aliphatic carbon content - High oxygen content - Medium ash content	Post-consumer shredded stream of multilayer cardboard/plastic for food packaging after certain fraction of the paper-based layer has been removed. Form: Pellets.
Cable Plastics (CP)	PE, PP, PVC. (Others: PET, Natural Rubber)	- High aliphatic carbon content - High chlorine content - Rich in ash	Non-separated waste from cable stripping. Only metals were sorted out previously. Form: Chopped pieces.
Textiles (TXT)	PET, PA, Polyacrylonitrile, Cellulose (Others: Wool, PVC, PU)	- Complex polymer blends - Low aliphatic carbon content - High heteroatom content	Textile waste after sorting the useful pieces of cloth. Form: Pellets.
Automotive Shredder Residue (ASR)	PP, PS, PU, Cellulose, PVC (Others: Tire Rubber, Acrylonitrile butadiene styrene (ABS), PC, PE, PAN, PMMA)	- Low polyolefin content - High aromatics content - Rich in heteroatoms - Rich in ash	Shredder Residue (SR) from the automotive and electrical waste (WEEE) sorting process. Form: Pellets.

PA, polyamide; PAN, polyacrylonitrile; PC, polycarbonate; PE, polyethylene; PP, polypropylene; PS, polystyrene; PU, polyurethane; PVC, polyvinyl chloride; PET, polyethylene terephthalate.

Table 4. Elemental compositions (%w_{dry}) and respective percent errors (%Err) for the materials used.

Element	CRB		CP		TXT		ASR 1		ASR 2	
	%w _{dry}	%Err	%w _{dry}	%Err	%w _{dry}	%Err	%w _{dry}	%Err	%w _{dry}	%Err
C	60.60	5.0	57.00	2.0	60.53	5.0	33.00	5.0	47.00	5.0
H	9.00	13.0	8.50	6.0	5.17	5.0	4.20	13.0	5.40	13.0
O*	21.00	15.5	0.66	12.5	29.97	5.0	13.66	10.7	13.17	10.7
N	0.35	29.0	0.02	6.0	2.90	6.0	1.30	29.0	1.60	29.0
S	0.07	10.0	0.02	6.0	0.09	9.1	0.33	10.0	0.19	10.0
Cl	0.20	25.0	5.80	6.0	0.12	7.6	0.51	25.0	0.64	25.0
Ash	8.75	11.0	28.00	3.0	1.22	15.9	47.00	11.0	32.00	11.0
LHV (MJ/kg)	30.14	5.0	27.20	7.2	28.13	7.4	13.90	15.0	20.10	15.0

*Calculated by difference-; LHV, low-heating value.

The main operational conditions used for **Papers I, II** and **III** in the DFB cracking reactor are indicated in Table 4. The rate of bed material circulation was approximately 15 tonnes/h. The cracker was fluidized with steam in a bubbling regime, the fuel residence time was estimated to be around 4–5 min, and the gas residence time was 5–10 s. The column titled “Feeding position” refers to Figure 7, whereby the cracker can be fed through two different ports. Position 6 is situated at the top of loop seal 1, which consists of an extruder in which the feedstock, in pellet or granulate form, is compressed and heated to obtain a molten flow that pours down onto the cracker bed. In position 8, the feedstock, also in pellet or granulate form, falls by gravity into the bed via a set of rotary valves working in an airlock system [42].

Table 5. Operational conditions used in the BFB cracking reactor for **Papers I, II** and **III**.

	Fuel	Temperature in Cracker (°C)	Bed material	Steam Flow (kg/h)	Material Flow (kg _{dry} /h)	Feeding Mode	Feeding Position	Steam/Fuel ratio
Paper I	PE	781; 787; 788; 793; 843	Silica Sand	120	90	Molten flow via extrusion	6	1.3
Paper II	PE	800	Silica Sand	120	90	Molten flow via extrusion	6	1.3
	CRB	805	Silica Sand	45	40	Molten flow via extrusion	6	1.1
	TXT	800	Silica sand	150	150	Top Feeding by gravity	8	1
	CP	800	Silica sand	130	108	Top Feeding by gravity	8	1.2
	ASR 1	790	Olivine	160	159	Top Feeding by gravity	8	1
	ASR 2	790	Olivine	160	157	Top Feeding by gravity	8	1
Paper III	PE	759–819	Silica Sand	45	64–91	Molten flow via extrusion	6	1.4–2.0

5. Results and Analysis

5.1. Parametric System Model Evaluation

From the experimental results obtained under the different operational conditions, the functions in Table 1 were tested, starting with the mono-parametric ones so as to satisfy the condition to keep the number of parameters for the function to a minimum. It was found that the topology of the mono-parametric functions was not sufficiently flexible to describe adequately the decaying behavior of the species. Therefore, at least one additional shape parameter was needed. As formulated in Equations (5)–(7), bi-parametric functions require at least three observables for each molecular system in order to derive a closed equation system that can determine the functions' parameters. This need was met through the results acquired for C4+ using the GC-VUV setup. Thus, the species that were evaluated to identify the shape parameters were C1, C2, and C3 for the paraffin function and C2, C3, and C4 for the olefin case. Figure 9 displays the functions that fit the experimental results. Out of the five experimental cases studied in **Paper I**, only three cases are shown, for the sake of clarity, based on their relevance to the process severity (defined as ethylene/propylene).

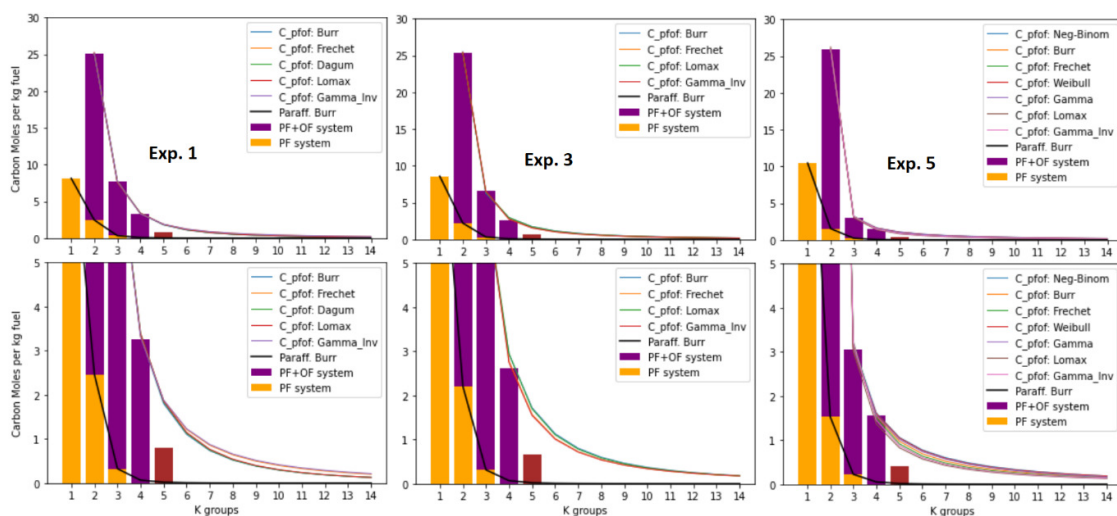


Figure 9. Results for some of the parametric functions tested in relation to the species' carbon distributions, expressed in $\text{molC}/\text{kg}_{\text{fuel}}$ vs. k -group, obtained for different severity cases (Experiments 1, 3 and 5, from left to right). The results are considered for the paraffin and olefin cases. Bottom row: Zoomed-in plots. (Red column: incomplete group species measured).

The bars in the upper row of Figure 9 show the experimental results for paraffin (orange bar) and the aggregated paraffins and olefins (purple bar), as well as the different functions that were tested to describe the systems. The designation 'pfof' refers to the summing of the paraffin and olefin functions for each k group. Notably, the heavy-tailed functions, which include Burr, Fréchet, Lomax, and Inverse Gamma, proved to be the most-flexible in terms of fitting the data across all severity levels. These functions exhibit elongated tails over longer carbon groups, leading to a lower rate of decay and an enlargement effect on their total enclosed areas, as shown in Table 6. This characteristic is especially crucial in low-severity cases, where the yields of long-chain species are still relevant. The function's tail and area correspond to the estimation done over the C5+ groups and the total estimated concentrations of such groups, respectively.

Table 6. Results for the total area, tail area (sum of C5+), and the parameters associated with the functions tested.

Function	Exp. 1				Exp. 3				Exp. 5			
	Area	Area Tail	α_1	α_2	Area	Area Tail	α_1	α_2	Area	Area Tail	α_1	α_2
Neg-Binomial	nan	nan	nan	nan	nan	nan	nan	nan	35.079	11.480	0.943	0.128
Con-Max	nan	nan	nan	nan	nan	nan	nan	nan	nan	nan	nan	nan
Burr*	40.048	10.742	1.204	1.117	40.323	13.025	1.243	0.867	36.204	12.574	1.620	0.465
Fréchet*	42.774	13.965	0.854	0.589	40.254	12.788	0.811	0.481	36.281	12.080	0.498	0.158
Dagum*	40.077	10.789	0.442	1.399	nan	nan	nan	nan	nan	nan	nan	nan
Gompertz	nan	nan	nan	nan	nan	nan	nan	nan	nan	nan	nan	nan
Weibull*	nan	nan	nan	nan	nan	nan	nan	nan	36.164	13.042	0.686	0.315
Gamma	nan	nan	nan	nan	nan	nan	nan	nan	34.500	10.594	0.066	0.126
Lomax*	40.134	10.865	2.538	1.380	40.335	12.994	1.949	0.691	35.713	11.120	1.444	0.076
Gamma_Inv*	43.458	14.631	0.760	0.429	40.438	12.940	0.744	0.342	36.122	11.622	0.439	0.061

*, Heavy-tailed functions; nan, No results.

At higher severities, the long chains progressively break down into shorter hydrocarbon species, contributing to the observed increase in data skewness. In such a scenario, topologies that feature rapid decay with relatively small estimated areas for the unmeasured groups, such as the Negative Binomial and Gamma functions (see Table 6), manage to accommodate the skewness of the data. Yet, the heavy-tailed functions mentioned earlier remained adaptable, effectively capturing the high-level skewness of the experimental data without significantly altering the total area. This result highlights the robustness of these types of functions for working in high- and low-severity scenarios.

Concerning the hydrogen distribution analysis, Figure 10 portrays the same experimental cases as presented before. The bottom-row plots provide detailed views of the experimental cases and the tested functions. The gray, blue, and purple-dashed curves represent the three theoretical scenarios: mono-enes (high), fully unsaturated (low), and fully conjugated (middle) cases of the olefin's Gamma effective function ($\gamma_{k,eff}^{of}$), respectively, as introduced in Equations (8)–(10). Notably, for the C7+ species, only the Burr, Fréchet, and Inverse Gamma functions remained within the permissible hydrogen range. These three functions consistently adhered to the hydrogen constraints for all the k-groups and experimental cases, indicating their shape's compatibility with the chemical characteristics of the olefin system. This alignment enhances confidence in the predictions made using such functions.

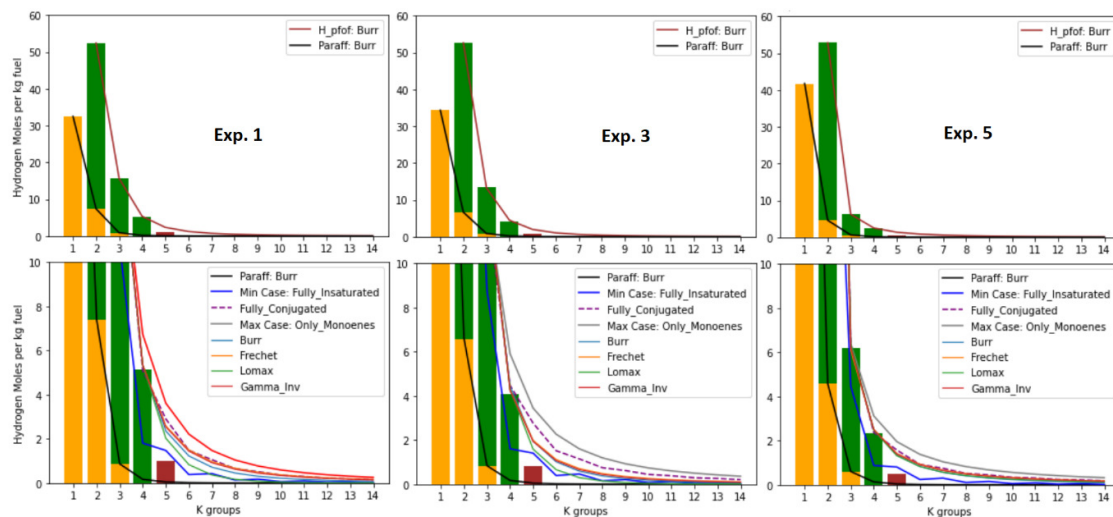


Figure 10. Results for the discriminated parametric functions applied to the hydrogen distribution of the species, expressed in molH/kg_{fuel} vs. k-group, for Experiments 1, 3 and 5. Upper row, Burr function results. Bottom row, zoom in and evaluation of the functions according with the gamma effective. (Red column: incomplete group species measured).

In Figure 9 and Figure 10, the C5 species bar is indicated in red, denoting incomplete species data due to equipment limitations. Only two out of approximately ten potential olefin species could be measured with the characterization methodology used. This mismatch is evident in relation to the functions' estimation for the C5 group. Regarding the carbon case (Figure 9), regardless of the function considered, there is a noticeable gap of around 100% of the C5 bar's height. This effect is particularly pronounced in the low-severity cases. Therefore, the study in **Paper I** underscores the model's predictive capabilities for the unmeasured carbon groups. These predictions remain physically consistent owing to the highly constrained framework established by the set of chemical and mathematical considerations applied to the system. Thus, in the absence of specific measurements for C5+ species, the PSM emerges as an important and useful tool for physically congruent estimations of these unmeasured species.

5.2. Parametric System Model Validation and Data Quality Assessment

As described in Section 2.3, the model outcomes can be validated by calculating the BOT. Such validation can be used in two ways. First, by ensuring that the BOT calculated from the PSM estimations using Equation 11 aligns with the expected values given by Equation 13 using the results derived from the HTR reactor. Second, by deliberately introducing errors into the experimental results through modifications in the calibration curves. This dual validation strategy aims to assess both the accuracy of the model's estimations and its capabilities for evaluating the quality of the data by detecting errors in the measurements.

The strategy also serves to validate the functions further by testing them against the highly skewed scenario created by the miscalibrated data. There, Burr was the sole function that was able to fit the data while still satisfying all the system constraints. Consequently, due to its robust performance across all the tested cases in **Paper I**, Burr was the function that was recommended for PSM applications under the evaluated process conditions.

Table 7 presents the results of the BOT calculation from the HTR outcomes versus the PSM estimations for both the calibrated and the miscalibrated cases.

Table 7. Bed's oxygen transport (BOT) calculated from the HTR versus the value estimated from the model (PSM), for the calibrated case (left table) and the miscalibrated case (right table).

Calibrated Case			Miscalibrated Case	
BOT HTR	BOT PSM	%diff	BOT HTR	BOT PSM
8.27	8.91	7.74	15.62	5.49
10.8	9.52	11.85	16.48	6.56
10.21	9.51	6.86	15.72	6.79
8.92	8.87	0.56	14.23	5.68
8.14	7.18	11.79	17.18	8.24

From the calibrated case in Table 7, it is shown that the BOT estimated by PSM presents an error of less than 12% with respect to the HTR values. This is a reasonable margin of error, given the unavoidable variations that occur in a large-scale process such as that used in these experiments, as well as the intrinsic numerical uncertainty of the model when predicting the carbon and the hydrogen tails.

In the miscalibrated case shown in Table 7, there is clear inconsistency in the results: the BOT calculated from the HTR results is 2–3-times higher than that estimated by the PSM. In this scenario, due to the topological constraints of the function's tail, the estimations of the total unknown species

of C5+ were such that there was no possibility to achieve alignment with the HTR case. This discrepancy strongly indicates a systematic error that affects the measurements, inflating the species yields and, consequently, producing a lower BOT value for the PSM estimation. This inflation of yields needs to be around 15% to ensure a match between the PSM and HTR calculations.

In situations where the origin of a discrepancy is unknown, potential errors can stem from various sources, including calibration inaccuracies linked to the analytical instruments, environmental fluctuations, and inadequate observation methods. In this case, the detection of species by the GC exceeded 100%vol in the measurement, indicating the presence of such errors in the overestimations of some species. Upon calculating the percentage difference for the miscalibrated species, the averaged discrepancy was approximately 10%, aligning with the magnitude of the PSM prediction (around 15%). This result underscores the ability of the PSM to pinpoint deficiencies in the quality of the experimental data. In future, PSM implementation could be further refined to assign errors specifically for each measured k-group, thereby enhancing the precision of the model's outcomes.

In general, the results demonstrate the potential of the PSM model to reduce the complexity of the measured systems, so as to transform an extensive list of experimentally determined species into just two parameters and shaping a specific distribution function. This reduction in degrees of freedom allows the PSM to capture and compress efficiently the information, with the possibility to enclose it in physics-informed frameworks, thereby enabling the acquisition of valuable insights. The findings highlight the potential of the PSM model as a versatile tool for improving measurement accuracy and for ensuring the statistical and chemical coherence of the results obtained from the steam cracking process. Furthermore, the estimation of C5+ carbon species constitutes a practical application for the downstream operations and controls of refineries.

5.3. Correlations between Product Distribution and Feedstock: Polymeric Composition Estimations

In the context of waste streams, as detailed in Section 3, the polymeric composition of the feedstock plays a crucial role in determining the distribution of the cracking product species. However, the materials investigated in **Paper II** were the rejected fractions of mechanical recycling with unknown and varied compositions. To estimate the polymeric composition, a numerical approach was introduced, as detailed in Section 3.1. The results of the feedstock composition estimations, based on Equations (17)–(22), are presented in Table 8.

Table 8. Estimated percentages for the materials' polymeric compositions.

	Solver	L. Function	PE	PP	Cell	PS	PET	PVC	PU	PA	ABS	PAN	NRubber	TRubber	Wool	PC
PE		<i>Expected (kg/kg_{feed})</i>	100													
	SCS	Fract_Err	43.40		35.64		7.85	0.36	3.90							
	SCS	Fract_Err	43.40	<0.01	35.64		7.85	0.36	3.90							
CRB	OSQP	Sum_Sqr	42.97	<0.01	35.23	<0.01	8.24	0.36	4.34	<0.01						
		<i>Average (kg/kg_f)</i>	43.25	<0.01	35.50	<0.01	7.98	0.36	4.05	<0.01						
		<i>Estimated (kg/kg_{feed})</i>	47.40	<0.01	38.91	<0.01	8.75	0.40	4.44	<0.01						
		<i>Expected (kg/kg_{feed})</i>	PE+PP > 40		< 50		5-12	< 1	PU+PA+PS < 5							
CP	SCS	Fract_Err	36.71	<0.01	<0.01	1.92	1.84	10.22	0.22					21.06		
	SCS	Fract_Err	36.37		<0.01	1.71	1.84	10.22	0.22					21.61		
	SCS	Fract_Err	37.24	<0.01		2.25	1.84	10.22	0.22					20.20		
		<i>Average (kg/kg_f)</i>	36.78	<0.01	<0.01	1.96	1.84	10.22	0.22					20.95		

		<i>Estimated (kg/kg_{daf})</i>	51.08	<0.01	<0.01	2.72	2.56	14.20	0.31			29.10	
		<i>Expected (kg/kg_{daf})</i>	Polef > 70			>10		PU+PA+PS < 2		Polef			
TXT	SCS	Fract_Err		7.08		69.42	0.22	<0.01	13.85	2.60	5.62		
	SCS	Fract_Err		7.11		69.44	0.22		13.83	2.64	5.54		
	OSQP	Fract_Err		7.06		69.59	0.22	<0.01	13.55	2.74	5.63		
	<i>Average (kg/kgf)</i>			7.08		69.48	0.22	<0.01	13.74	2.66	5.60		
	<i>Estimated (kg/(kg/kg_{daf}))</i>			7.17		70.34	0.22	<0.01	13.91	2.69	5.67		
		<i>Expected (kg/(kg/kg_{daf}))</i>	< 15		> 60	< 1	PU+PA+PAN 10-20		< 10				
ASR 1	SCS	Fract_Err	12.51	21.75	<0.01	0.90	13.67	<0.01	<0.01	3.84	<0.01		
	SCS	Fract_Err	12.51	21.75	<0.01	0.90	13.67	<0.01		3.84	<0.01		
	SCS	Fract_Err	12.51	21.75	<0.01	0.90	13.67			3.84	<0.01		
	<i>Average (kg/kgf)</i>		12.51	21.75	<0.01	<0.01	0.90	13.67	<0.01	<0.01	3.84	<0.01	<0.01
	<i>Estimated (kg/(kg/kg_{daf}))</i>		23.60	41.04	<0.01	<0.01	1.70	25.80	<0.01	<0.01	7.24	<0.01	<0.01
		<i>Expected (kg/kg_{daf})</i>	PP > 20, Polef > 30		> 10	< 2	PU+PA+PS >20	ABS+PC+PMMA <10		Polef			
ASR 2	SCS	Fract_Err	13.13	19.47	9.60	1.13	16.00	<0.01	<0.01	<0.01	8.67	<0.01	
	SCS	Fract_Err	13.07	19.48	9.66	1.13	15.98		<0.01		8.68	<0.01	
	SCS	Fract_Err	13.03	19.48	9.70	1.13	15.98				8.68	<0.01	
	<i>Average (kg/kgf)</i>		13.08	19.48	9.65	1.13	15.99	<0.01	<0.01	<0.01	8.68	<0.01	<0.01
	<i>Estimated (kg/kg_{daf})</i>		19.23	28.64	14.20	1.66	23.51	<0.01	<0.01	<0.01	12.76	<0.01	<0.01
		<i>Expected (kg/kg_{daf})</i>	PP > 20, Polef > 30		> 10	< 2	PU+PA+PS >20	Other alloys <5-10		Polef			

Polef, PE+PP+Rubber; daf: dry ash-free feedstock. ABS; acrylonitrile butadiene styrene; PA, polyamide; PAN, polyacrylonitrile; PC, polycarbonate; PE, polyethylene; PMMA, polymethyl methacrylate; PP, polypropylene; PS, polystyrene; PU, polyurethane; PVC, polyvinyl chloride; PET, polyethylene terephthalate.; SCS, Splitting Conic Solver; OSQP, Operator Splitting Quadratic Program.

Overall, the estimates presented in Table 8 exhibit a reasonable degree of approximation. The residuals for the elemental balances, obtained from the optimization, present an averaged total error of <2% across all the materials. For the LHV case, the averaged error is less than 10%, except for the textiles case, where it reaches 17%. However, this deviation is deemed to be reasonable due to the pure-components approximation used, as well as the presence of additional polymers and additives that are commonly found in such waste streams. Moreover, the estimates fall within the expected share ranges for each polymer component, which were determined through visual pre-identification of the material, common material production composition, and/or rough elemental estimations.

Figure 11 displays a graphical summary of the estimated mass fractions of the different polymers in the evaluated materials presented in Table 8.

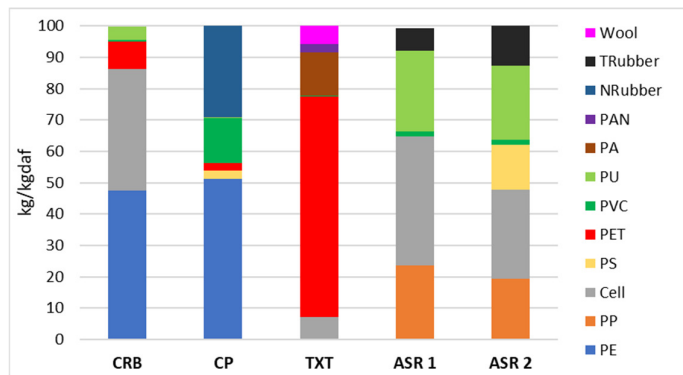


Figure 11. Summary of estimated polymeric mass fractions in kg/kg_{daf} for the evaluated materials.

5.4. Correlations between Product Distribution and Feedstock: Carbon Bond-Based Classification Evaluation

The compiled results from the thermal cracking experiments performed under the conditions described in Table 5 for the evaluated materials in Paper II are shown in Figure 12.

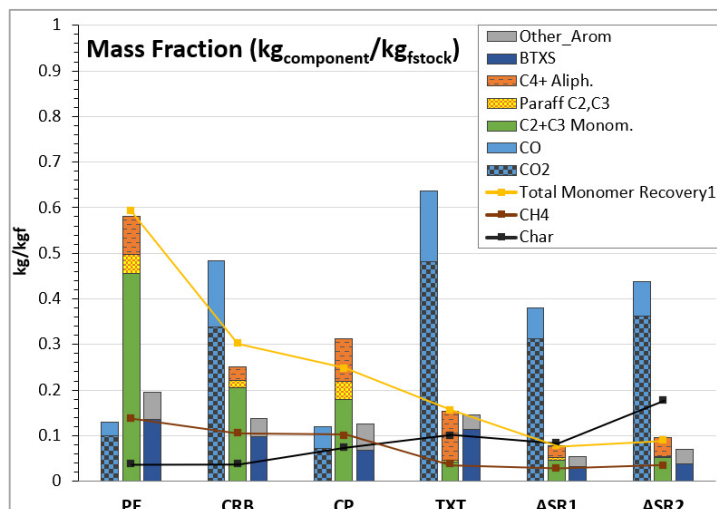


Figure 12. Results of the cracking DFB process for the evaluated materials in terms of mass ratio (kg/kgf). Total Monomer Recovery = C2+C3 (Monomers) + BTXS.

Based on the carbon bond classification rules described in Section 3.2, the carbon atoms within the polymeric components of the feedstock were categorized based on their specific bond types. These categories were then aggregated in accordance with their corresponding estimated polymeric proportions for each material (Table 8). Here, the C-X group was further subdivided into C-O (carbons bonded to oxygen atoms) and C-Xh (carbons attached to other heteroatoms). In those cases in which a carbon was bonded to multiple types of heteroatoms, preference was given to oxygen, due to its greater tendency to form carbon products, such as CO and CO₂, during the process. The classification approach is illustrated in Figure 13 (left panel) in terms of the carbon ratios for each of the bond groups, calculated in relation to the respective feedstock carbon contents. In parallel, Figure 13 (right panel) displays the carbon ratios of the respective thermal-cracking product yields, sorted according to the corresponding classification criteria.

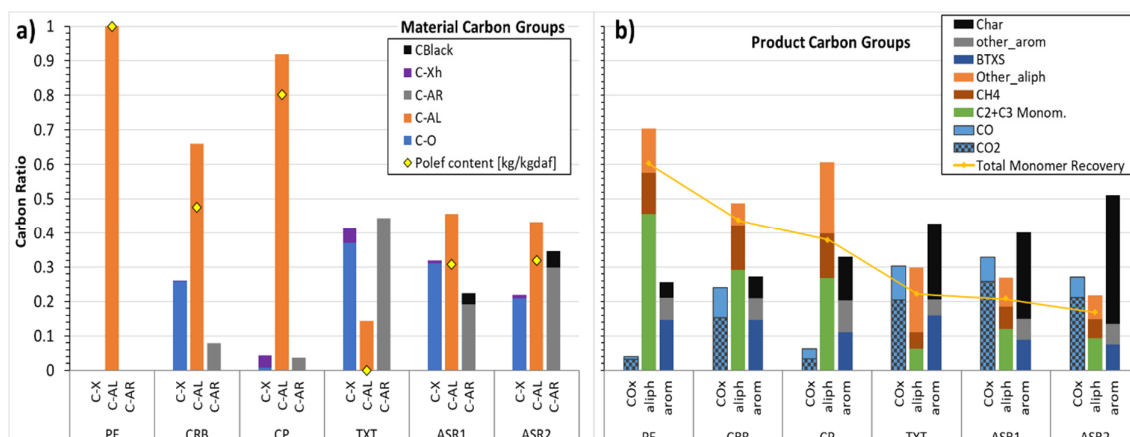


Figure 13. Carbon ratios of each material's composition before (panel a) and after (panel b) thermal cracking conversion. The carbons are classified into three groups: C-X, C-AL and C-AR groups for the original material composition; and CO_x, aliphatics and aromatics for the cracking products.

In Figure 13, the variations obtained for the defined carbon groups under cracking conditions are evident. The polymer composition estimates in Table 8, coupled with knowledge of the cracking products from the carbon bond-based classification framework, provide important insights into key aspects of carbon conversion within the process. CRB, TXT, and ASR, which contain substantial amount of C-O bonds due to their high share of either Cell or PET (Figure 13, left panel), yield notable CO_x levels, as compared with CP, which completely lacks C-O bonds in its structure.

However, the levels of CO_x produced from CRB and TXT are lower than their respective levels of C-O. This suggests that part of the carbon in the C-O bonds, originating from ether or ester linkages in Cell or PET, respectively, are converted into species other than CO_x, such as aliphatics, aromatics/polyaromatics or char. As an example, TXT is primarily made of PET, which lacks C-AL due to the ester linkages in its structure. Despite the low C-AL levels (~14%), conversion results in double production of aliphatics, primarily C₄+, considering the original C-AL levels. This outcome reveals that the ester oxygen connecting the terephthalate with the ethylene in the PET structure is more likely to leave with the carbonyl (later to produce CO₂) than to cause the C-C bond to break. This explains the decrease in CO_x relative to C-O and the increase in aliphatics in relation to C-AL. These results mean that the ethylene carbon in PET may be better-placed in the C-AL group than in C-O, constituting an exception to the carbon assignment rule. On the other hand, ASR, which has a lower oxygen content than TXT, exhibits higher CO_x levels post-cracking, a result that is attributed to ash-induced oxygen transport in the DFB system, as detailed by Pissot et al. [43].

In terms of the aliphatics group (C-AL), CRB and CP, which are rich in polyolefins (47% and 80%, respectively) with linear aliphatic bonds and, thus, showing the highest C-AL levels, gave the highest level of olefin-monomer recovery, even comparable to pure PE. Aligned with this, ASR, with a higher linear polyolefins content than TXT, showed a relatively higher level of olefin-monomer conversion compared with TXT.

Regarding the aromatic compounds, two main mechanisms of formation were observed across the materials: thermal decomposition of polymers that contain aromatic structures, and aromatization through the cyclization of cracking reaction precursors, leading to the production of monoaromatics and polyaromatics. TXT exhibited the highest level of conversion to BTXS (16%) due to its PET composition being rich in aromatic structures. Nonetheless, the nearly identical levels of C-AR with the produced aromatics for TXT suggest that either all the carbons in C-AR remained as carbons within a ring in the products or there was a near-zero total inter-group conversion to aromatics. On the other hand, the high-polyolefin materials, such as PE, CRB, and CP, despite lacking aromatic groups on their original structure, showed a significantly large aromatics fraction, indicating formation through cyclization reactions.

Overall, the BTXS/polyaromatics ratio was higher for the materials that contained aromatics in their structures, e.g., TXT, CRB and ASR, indicating that decomposition rather than cyclization mechanisms predominantly yield the valuable monomeric BTXS fraction. On the other hand, a significant polyaromatics yield was observed for materials with high polyolefin contents, indicating the further development of uncontrolled cyclization reactions. Notably, CP displayed the largest polyaromatics fraction among the materials, indicating the occurrence of significant secondary reactions during cracking. Chloride-containing polymers, such as PVC, facilitate aromatization in the dechlorination process through increased double-bond and conjugated diene formation [26], which are precursors for cyclization reactions. In this regard, the active dienophile participation of ethylene and propylene in Diels-Alder reactions is evidenced by the CP's reduced carbon share of olefin monomers.

Concerning char formation during thermal cracking, the polyolefin-rich materials such as CRB and CP yielded limited levels of char (6% and 13%, respectively), whereas TXT and ASR produced higher char yields. TXT char and ASR char arise from excessive aromatization that is induced by the highly heterogeneous composition along with additives and from carbon-based fillers, as in the case of ASR. Char, which stays in the reactor and then leaves along with the sand, contributed to heat production in the combustor or was filtered out from the raw gas (when produced in form of soot). It is pertinent to note that in the utilized DFB system, the amount of char produced did not significantly influence the system's overall heat balance due to the continuous operation of the biomass-based, full-scale boiler.

A cross-correlations analysis between the feedstock and the cracking products for the defined carbon bond group classification is illustrated in Figure 14. In this figure, the x-axis corresponds to the feedstocks' carbon fractions of C-O, C-AL, and C-AR (plots **a**, **b**, and **c**, respectively), while the y-axis represents the level of carbon conversion into the evaluated carbon product species in each plot.

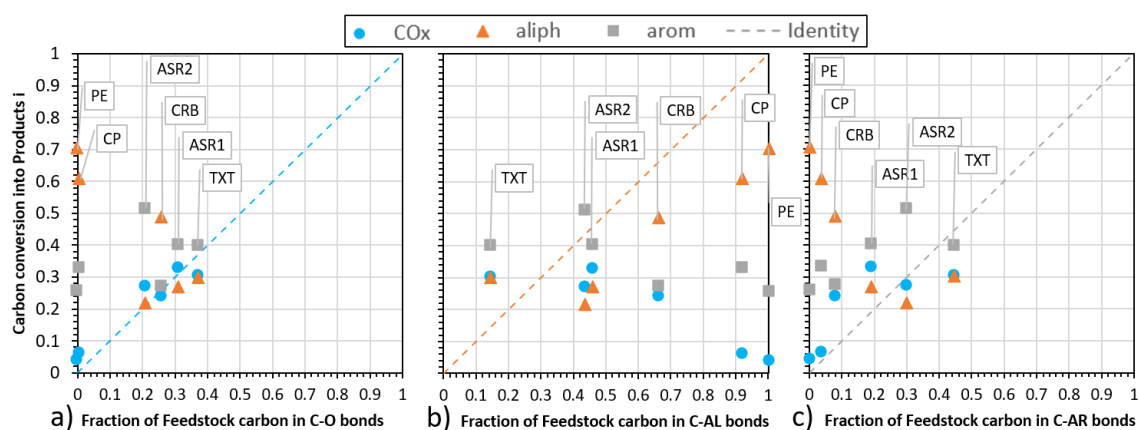


Figure 14. Carbon conversion into product compound i (kgC of species i in product per kgC in feedstock) as a function of the fraction of the carbon bond group j in the feedstock (kgC in bond type j per kgC in feedstock). Carbon Bond group j = C-O, C-AL, C-AR; product compound i = COx, aliphatics, aromatics.

In the plot **a** of Figure 14, a positive and seemingly linear correlation between COx (blue markers) and C-O carbons is evident, starting above the dashed diagonal line, reflecting the inherent oxygen interaction in the system due to the steam environment. A similar positive correlation with C-AR carbons is observed in plot **c**. Conversely, plot **b** shows an overall negative correlation with the aliphatic bonded carbons (C-AL), corresponding to the decrease in the feedstock oxygen content. The COx starts from around 0.3 for C-AL levels <0.5 and thereafter declines, reaching the level of pure PE (~ 0.05).

Plot **b** in Figure 14 illustrates a positive correlation between aliphatics (orange markers) and C-AL, as expected. In plot **a**, there is a negative correlation with C-O, since such bonds instead tend to end up as COx species. The correlation of aliphatics with C-AR is also negative (see plot **c**), indicating the low likelihood of ring opening to form linear structures. On the other hand, in plots **a** and **c**, the aromatics (gray markers) show slightly positive correlations with C-AR and C-O, respectively, albeit slightly negative correlations with C-AL (plot **b**, suggesting the still-significant formation of ring structures by cyclization even when the original material lacks such structures).

Apparent deviations from linearity are observed for TXT in all the plots. This is likely due to its low polyolefin content, though mainly due to the conversion of other groups, especially certain C-O carbons that are assigned according to the bond classification rules into aliphatic species during the

cracking process, as explained previously. This effect causes the TXT to behave as an outlier case in all the plots in Figure 14, and provides another indication that the C-O assignment rule must be revised for cases such as this in order to deal with such behavior.

Individual species and groups, such as olefin C2 and C3 monomers and BTXS, can be analyzed in a manner similar to that used in Figure 14. In Figure 15, these species are plotted against C-AL (plot **a**) and C-AR (plot **b**), providing insights into potential correlations. Methane is also included in the plot for illustrative purposes.

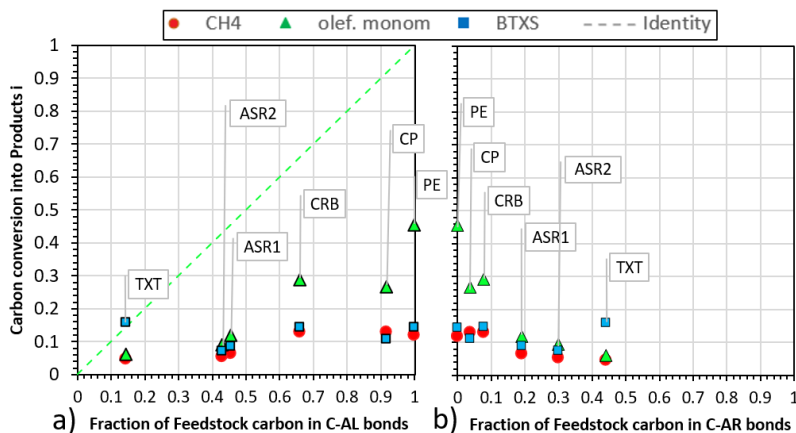


Figure 15. Carbon conversion into product compound i (kgC of species i in product per kgC in feedstock) as a function of the fraction of the carbon bond group j in the feedstock (kgC in bond type j per kgC in feedstock). Carbon bond group $j = C-AL, C-AR$; product compound $i = CH_4, olefin\ monomers, BTXS$.

Plots **a** and **b** in Figure 15 reveal distinct trends for olefin monomers (green markers) concerning C-AL and C-AR, respectively. A clear positive correlation is seen with aliphatic carbon bonds (C-AL), indicating the persistence of aliphatic bonds to stay as aliphatic chains, despite the seemingly random radical-based breakage that they undergo during the process. The correlation shifts towards lower values compared to the total aliphatics in Figure 14 (plot **b**), which aligns closer to the identity line. This shift stems from C-AL being utilized to produce other aliphatic components (e.g., CH_4 and others). Nonetheless, the trend remains similar to that of the aliphatics, suggesting a strong tendency for C-AL to produce valuable C2 and C3 monomers under the evaluated process conditions. In contrast there is a nonlinear negative correlation for the aromatic carbons (C-AR), indicating once again the minimal likelihood of the ring structures to break down and contribute to the olefin monomeric yield. Methane (red markers) exhibits a slightly positive correlation with C-AL, and a slightly negative correlation with C-AR.

BTXS (blue markers) shows no definitive trends for any of the two bond groups, remaining relatively stable at around 0.15. Interestingly, the positive correlation between aromatics and C-AR bonds observed in Figure 14 (plot **c**) is lost for BTXS in Figure 15 (plot **b**). This lack of correlation for one-ring aromatics suggests multiple routes for their production, with no clear predominant source. As discussed earlier, some of the evaluated materials predominantly follow the cyclization route, such as high-polyolefin materials, while others yield aromatics through direct detachment of existing aromatic rings, as observed for TXT.

The carbon bond-based classification method offers an approach from a data perspective to generalize the complexity of feedstock polymeric blends. It provides a simplified way to assess for cracking processes the impacts of specific chemical structures in a feedstock on the carbon product distribution.

Although further refinements to the classification rules are needed, especially concerning materials such as TXT that have observed non-linear behaviors, these preliminary correlations create useful mappings of defined carbon bond groups pre- and post-cracking. Overall, the developed framework concept paves the way for more-advanced, predictive, two-way models that consider more materials, such that the correlations not only be useful for estimating certain carbon groups (or potential monomer recovery) based on feedstock and process conditions, but also for defining polymeric compositions based on the key species and/or carbon groups observed in the product distribution.

6. Future Research Perspectives

Considering the control and optimization of the cracking conversion process for a heterogeneous polymeric feedstock, it is of the utmost importance to have online knowledge of the feedstock composition entering in the reactor at all times, so as to optimize the process towards an economically favorable species distribution. The numerical method of estimation presented in this work constitutes a useful and rapid way to obtain such quantification.

In that regard, the system bond classification framework can help to refine the numerical estimation of the polymer's share. As described in Section 3.1, Equation (17) provides a system of equations that allows to numerically estimate the polymeric shares based on the elemental and energy balances. Each equation added to the system is an additional constraint layer that is designed to restrict the solution space created by all the possible polymer sets.

The classification framework may constitute an additional set of equations that adds one more level of restriction to the system. This new constraint layer is of high relevance because it can link the measured cracking products to the respective polymeric estimations. To present the concept briefly, the yields obtained for each product group can be seen as a linear combination of the conversion that each carbon-bond group underwent into that particular product group during the cracking process. In mathematical form, considering a polymer component j , for a defined set of carbon bond groups $\{b\}$ and product groups $\{g\}$, the carbon mass fraction $y_c^{g,j}$ of the product group g can be defined by Equation (23):

$$y_c^{g,j} = \sum_b y_{c,b}^{g,j} \quad (23)$$

Here, $y_{c,b}^{g,j}$ must be read as the carbon mass fraction of the bond b that was converted into group g for component j . For the case studied in this work, $b \in \{C-O, C-Al, C-Ar\}$ and $g \in \{COx, aliph, arom\}$. Thus, Equation (23) can be rewritten as Equation (24):

$$y_c^{g,j} = y_{c,C-O}^{g,j} + y_{c,C-Al}^{g,j} + y_{c,C-Ar}^{g,j} \quad (24)$$

$$\Rightarrow y_c^{g,j} = \beta_{c,C-O}^{g,j} y_c^{C-O,j} + \beta_{c,C-Al}^{g,j} y_c^{C-Al,j} + \beta_{c,C-Ar}^{g,j} y_c^{C-Ar,j} = \beta_{c,b}^{g,j} y_c^{b,j} \quad (E.N) \quad (25)$$

The term $y_c^{b,j}$ corresponds to the carbon mass fraction of the bond b in component j and $\beta_{c,b}^{g,j}$ is defined as the conversion coefficient that relates the fraction of bonds b in component j that were converted to group g . So, each product group g corresponds to the sum of all the fractional contributions of each of the defined bonds b to that particular product group. Then, Equation (25) expresses the carbon mass fraction of the group g ($y_c^{g,j}$), as a function of $y_c^{b,j}$. Based on this, $\beta_{c,b}^{g,j}$ can be defined as a conversion tensor that represents the cracking process, connecting the bonds found in the feedstock with the final product groups.

Ideally, each measured product g coming from a feedstock f would correspond to the contributions of all the groups g provided by the polymeric components contained in the feedstock. For a fuel with a set of polymeric components $j \in \{PE, PP, PVC, \dots\}$, this can be expressed by multiplying $y_{c,j}^g$ (j was transposed) by the mass fraction vector $x^{j,f}$ of Equation (17). However, in reality, the presence of certain polymers in the feedstock blend might cause cross-interactions between the products released by other polymers. In its simplest form, this could be approximated by adding a correction term ($\epsilon_b^g \in (-1,1)$) to the conversion tensor $\beta_{c,b}^{g,j}$, as is expressed in Equation (26). Thus, for a fuel with a set of

polymeric components $j \in \{PE, PP, PVC, \dots\}$, the carbon mass fraction of the measured group g when feedstock f is converted can be defined by Equation (27):

$$\hat{y}_{c,j}^g = (\beta_{c,b}^{g,j} + \epsilon_b^g) y_c^{b,j} = \hat{\beta}_{c,b}^{g,j} y_c^{b,j} \quad (E.N) \quad (26)$$

$$\hat{y}_{c,j}^g x^{j,f} = y_c^{g,f} \quad (E.N) \quad (27)$$

where $\hat{y}_{c,j}^g$ corresponds to the corrected carbon mass fraction of group g in component j and $y_c^{g,f}$ the measured carbon mass fraction of group g of the feedstock f . Equation (27) will then constitute an additional set of $size\{g\}$ equations, which can be added to the system defined in Equation (17).

On the other hand, an important synergy can be generated with the PSM features, as it can always help to provide an assessment on the cracking data, so as to improve its quality and/or predictive accuracy for key species.

Figure 16 presents a schematic of the integration of the model and its application for backward estimations of polymer compositions.

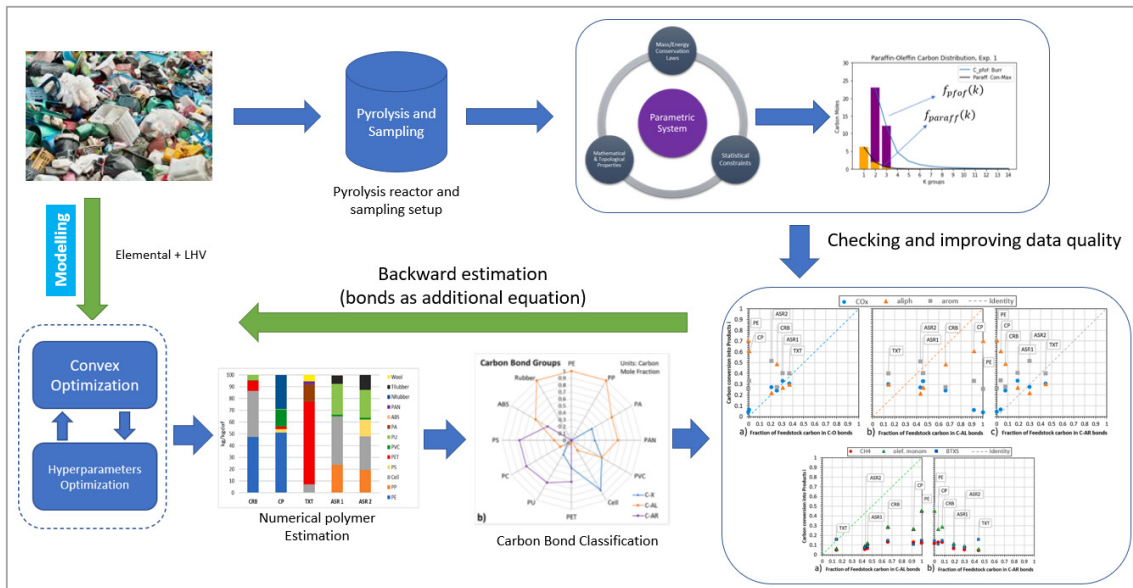


Figure 16. Integration of the PSM and carbon bond-based classification models.

7. Conclusions

This thesis presents the results of research efforts to develop data analysis models that can be used as tools to enhance the understanding and processing of data generated from the thermal cracking conversion of polymeric feedstocks. These tools incorporate specific chemical and mathematical characteristics of the conversion system, enabling the extraction of meaningful and physically consistent information from the process data.

The cracking product species distribution is a key focus in the two models presented in this work. The models were developed by evaluating the data in two ways. First, the species outcomes were described in a special data representation using a framework constituted by the chemical and mathematical characteristics of the system. Based on this, predictions of unknown species quantities and data quality assessments could be performed. Second, the product species and information on the feedstock polymeric composition were considered in a novel carbon bond-based classification framework, as to the basis for exploring and mapping correlations between the relevant data for the carbon groups pre- and post-cracking of the plastics mixtures.

The first model consisted of a Parametric System Model (PSM), which was developed to represent the product species data emerging from the cracking process. This model was defined within a framework that contained generic knowledge of the evaluated chemical system in terms of conservation laws and probabilistic properties. By including elemental carbon, hydrogen and oxygen balances and a topology that is statistically meaningful, the model proved effective in compressing the species' carbon and hydrogen data into a special bi-parametric function. The model enabled physically consistent estimations of unmeasured carbon group species, addressing the constraints linked to the characterization equipment and identified experimental data errors, thereby showcasing its potential for data quality assessments.

The second model involved evaluation of the product composition coming from the cracking of highly heterogeneous feedstocks, represented by four different post-consumer waste-derived materials. Here, correlations between the cracking products and the feedstock composition were studied, based on a carbon bond-based classification system that classified the carbons in aliphatic (C-AL), aromatic (C-AR), and heteroatom-bonded (C-X; X=O, N, S, Cl) structures.

Among the main findings, visible correlations were found between the defined feedstock structures and the products chemical groups. For instance, a positive linear correlation was observed between the carbons in the feedstock bonded to oxygen (C-O) and the CO_x product species yield, contrasting with a negative correlation to C-AL. A slightly positive correlation was seen between the aromatics and C-AR in the feedstock, whereas there was a negative correlation with C-AL, indicating the stability of the aromatic rings in terms of tending to remain in ring form rather than break down into chains. No definitive trend emerged for BTXS concerning the defined carbon-bond groups.

Overall, the observed capabilities of PSM position the model as a tool to assess and enhance the quality of the measurements obtained from the cracking process. In addition, the developed carbon bond-based classification system provides a unique common framework that enables trend identification and potential mapping between feedstock polymeric characteristics with the respective conversion process outputs. Both models can eventually work together in a synergistic way to unlock deeper insights into the polymer steam-cracking process, paving the way for more-advanced predictive models and valuable applications in the control and optimization of this type of sustainable waste transformation process.

8. References

- [1] Global Plastics Outlook, OECD, 2022. <https://doi.org/10.1787/de747aef-en>.
- [2] <https://stat.link/elpign>, OECD (2022).
- [3] OECD, Lifecycle of plastic waste worldwide in 2019 (in million metric tons)[graph], (2019).
- [4] F. Kähler, M. Carus, C. vom Berg, M. Stratmann, CO₂ Reduction Potential of the Chemical Industry Through CCU, 2022. <https://doi.org/10.52548/UTRL5869>.
- [5] M. Rosental, T. Fröhlich, A. Liebich, Life Cycle Assessment of Carbon Capture and Utilization for the Production of Large Volume Organic Chemicals, *Frontiers in Climate 2* (2020). <https://doi.org/10.3389/fclim.2020.586199>.
- [6] H. Thunman, T. Berdugo Vilches, M. Seemann, J. Maric, I.C. Vela, S. Pissot, H.N.T. Nguyen, Circular use of plastics-transformation of existing petrochemical clusters into thermochemical recycling plants with 100% plastics recovery, *Sustainable Materials and Technologies 22* (2019) e00124. <https://doi.org/10.1016/j.susmat.2019.e00124>.
- [7] E. Commission, J.R. Centre, P. Garcia-Gutierrez, A. Amadei, D. Klenert, S. Nessi, D. Tonini, D. Tosches, F. Ardente, H. Saveyn, Environmental and economic assessment of plastic waste recycling – A comparison of mechanical, physical, chemical recycling and energy recovery of plastic waste, Publications Office of the European Union, 2023. <https://doi.org/doi/10.2760/0472>.
- [8] M.A. Fox, J.K. Whitesell, *Organic Chemistry*, Jones and Bartlett Publishers, 2004. https://books.google.se/books?id=xx_uIP5LgO8C.
- [9] T. Larraín, M. Carrier, L.R. Radovic, Structure-reactivity relationship in pyrolysis of plastics: A comparison with natural polymers, *J Anal Appl Pyrolysis 126* (2017) 346–356. <https://doi.org/10.1016/j.jaap.2017.05.011>.
- [10] J. Weitkamp, Catalytic Hydrocracking—Mechanisms and Versatility of the Process, *ChemCatChem 4* (2012) 292–306. <https://doi.org/10.1002/cctc.201100315>.
- [11] A. de Klerk, Thermal Cracking of Fischer–Tropsch Waxes, *Ind Eng Chem Res 46* (2007) 5516–5521. <https://doi.org/10.1021/ie070155g>.
- [12] S. Chakraborty, Generating discrete analogues of continuous probability distributions-A survey of methods and constructions, *J Stat Distrib Appl 2* (2015) 6. <https://doi.org/10.1186/s40488-015-0028-6>.
- [13] S. Coles, *An Introduction to Statistical Modeling of Extreme Values*, Springer London, London, 2001. <https://doi.org/10.1007/978-1-4471-3675-0>.
- [14] T. Berdugo Vilches, J. Marinkovic, M. Seemann, H. Thunman, Comparing Active Bed Materials in a Dual Fluidized Bed Biomass Gasifier: Olivine, Bauxite, Quartz-Sand, and Ilmenite, *Energy & Fuels 30* (2016) 4848–4857. <https://doi.org/10.1021/acs.energyfuels.6b00327>.
- [15] M. Israelsson, A. Larsson, H. Thunman, Online Measurement of Elemental Yields, Oxygen Transport, Condensable Compounds, and Heating Values in Gasification Systems, *Energy & Fuels 28* (2014) 5892–5901. <https://doi.org/10.1021/ef501433n>.

- [16] Supriyanto, P. Ylittero, T. Richards, Gaseous products from primary reactions of fast plastic pyrolysis, *J Anal Appl Pyrolysis* 158 (2021) 105248. <https://doi.org/10.1016/j.jaap.2021.105248>.
- [17] S.C. Moldoveanu, General information about pyrolysis, in: *Analytical Pyrolysis of Natural Organic Polymers*, Elsevier, 2021: pp. 3–27. <https://doi.org/10.1016/B978-0-12-818571-1.00001-7>.
- [18] M.S. Abbas-Abadi, Y. Ureel, A. Eschenbacher, F.H. Vermeire, R.J. Varghese, J. Oenema, G.D. Stefanidis, K.M. Van Geem, Challenges and opportunities of light olefin production via thermal and catalytic pyrolysis of end-of-life polyolefins: Towards full recyclability, *Prog Energy Combust Sci* 96 (2023) 101046. <https://doi.org/10.1016/j.pecs.2022.101046>.
- [19] W. Kaminsky, M. Predel, A. Sadiki, Feedstock recycling of polymers by pyrolysis in a fluidised bed, *Polym Degrad Stab* 85 (2004) 1045–1050. <https://doi.org/10.1016/J.POLYMDEGRADSTAB.2003.05.002>.
- [20] M.S. Abbas-Abadi, The effect of process and structural parameters on the stability, thermo-mechanical and thermal degradation of polymers with hydrocarbon skeleton containing PE, PP, PS, PVC, NR, PBR and SBR, *J Therm Anal Calorim* 143 (2021) 2867–2882. <https://doi.org/10.1007/s10973-020-09344-0>.
- [21] Y. Liu, J. Qian, J. Wang, Pyrolysis of polystyrene waste in a fluidized-bed reactor to obtain styrene monomer and gasoline fraction, *Fuel Processing Technology* 63 (2000) 45–55. [https://doi.org/10.1016/S0378-3820\(99\)00066-1](https://doi.org/10.1016/S0378-3820(99)00066-1).
- [22] M. Herrera, G. Matuschek, A. Kettrup, Main products and kinetics of the thermal degradation of polyamides, *Chemosphere* 42 (2001) 601–607. [https://doi.org/10.1016/S0045-6535\(00\)00233-2](https://doi.org/10.1016/S0045-6535(00)00233-2).
- [23] M. Nielsen, P. Jurasek, J. Hayashi, E. Furimsky, Formation of toxic gases during pyrolysis of polyacrylonitrile and nylons, *J Anal Appl Pyrolysis* 35 (1995) 43–51. [https://doi.org/10.1016/0165-2370\(95\)00898-0](https://doi.org/10.1016/0165-2370(95)00898-0).
- [24] H. Zhou, C. Wu, J.A. Onwudili, A. Meng, Y. Zhang, P.T. Williams, Influence of process conditions on the formation of 2–4 ring polycyclic aromatic hydrocarbons from the pyrolysis of polyvinyl chloride, *Fuel Processing Technology* 144 (2016) 299–304. <https://doi.org/10.1016/J.FUPROC.2016.01.013>.
- [25] N. Miskolczi, L. Bartha, A. Angyal, Pyrolysis of Polyvinyl Chloride (PVC)-Containing Mixed Plastic Wastes for Recovery of Hydrocarbons, *Energy & Fuels* 23 (2009) 2743–2749. <https://doi.org/10.1021/ef8011245>.
- [26] J. Zhou, G. Liu, S. Wang, H. Zhang, F. Xu, TG-FTIR and Py-GC/MS study of the pyrolysis mechanism and composition of volatiles from flash pyrolysis of PVC, *Journal of the Energy Institute* 93 (2020) 2362–2370. <https://doi.org/10.1016/j.joei.2020.07.009>.
- [27] J. Scheirs, W. Kaminsky, eds., *Feedstock Recycling and Pyrolysis of Waste Plastics: Converting Waste Plastics into Diesel and Other Fuels*, Wiley, 2006. <https://doi.org/10.1002/0470021543>.
- [28] C. Mandviwala, T. Berdugo Vilches, M. Seemann, R. Faust, H. Thunman, Thermochemical conversion of polyethylene in a fluidized bed: Impact of transition metal-induced oxygen

- transport on product distribution, *J Anal Appl Pyrolysis* 163 (2022).
<https://doi.org/10.1016/j.jaap.2022.105476>.
- [29] S. Masoumeh Safavi, C. Richter, R. Unnthorsson, Dioxin and Furan Emissions from Gasification, in: *Gasification [Working Title]*, IntechOpen, 2021.
<https://doi.org/10.5772/intechopen.95475>.
- [30] J. Maric, T. Berdugo Vilches, S. Pissot, I. Cañete Vela, M. Gyllenhammar, M. Seemann, Emissions of dioxins and furans during steam gasification of Automotive Shredder residue; experiences from the Chalmers 2–4-MW indirect gasifier, *Waste Management* 102 (2020) 114–121. <https://doi.org/10.1016/j.wasman.2019.10.037>.
- [31] X. Wu, J. Li, L. Yao, Z. Xu, Auto-sorting commonly recovered plastics from waste household appliances and electronics using near-infrared spectroscopy, *J Clean Prod* 246 (2020) 118732. <https://doi.org/10.1016/j.jclepro.2019.118732>.
- [32] U.K. Adarsh, E. Bhoje Gowd, A. Bankapur, V.B. Kartha, S. Chidangil, V.K. Unnikrishnan, Development of an inter-confirmatory plastic characterization system using spectroscopic techniques for waste management, *Waste Management* 150 (2022) 339–351. <https://doi.org/10.1016/j.wasman.2022.07.025>.
- [33] B. O’Donoghue, Operator splitting for a homogeneous embedding of the linear complementarity problem, (2020). <https://doi.org/10.48550/arxiv.2004.02177>.
- [34] SCS — SCS 3.2.1 documentation, (n.d.). <https://www.cvxgrp.org/scs/> (accessed October 12, 2022).
- [35] S. Diamond, S. Boyd, CVXPY: A Python-Embedded Modeling Language for Convex Optimization, *J. Mach. Learn. Res.* 17 (2016) 2909–2913.
- [36] E. Akca, A. Gursel, N. Sen, A review on devulcanization of waste tire rubber, *Periodicals of Engineering and Natural Sciences (PEN)* 6 (2018) 154. <https://doi.org/10.21533/pen.v6i1.167>.
- [37] D. Landi, S. Vitali, M. Germani, Environmental Analysis of Different End of Life Scenarios of Tires Textile Fibers, *Procedia CIRP* 48 (2016) 508–513. <https://doi.org/10.1016/J.PROCIR.2016.03.141>.
- [38] H. Zhou, A. Meng, Y. Long, Q. Li, Y. Zhang, Classification and comparison of municipal solid waste based on thermochemical characteristics, *J Air Waste Manage Assoc* 64 (2014) 597–616. <https://doi.org/10.1080/10962247.2013.873094>.
- [39] D. Neves, H. Thunman, L. Tarelho, A. Larsson, M. Seemann, A. Matos, Method for online measurement of the CHON composition of raw gas from biomass gasifier, *Appl Energy* 113 (2014) 932–945. <https://doi.org/10.1016/j.apenergy.2013.08.032>.
- [40] T. Berdugo Vilches, H. Thunman, Experimental Investigation of Volatiles–Bed Contact in a 2–4 MWth Bubbling Bed Reactor of a Dual Fluidized Bed Gasifier, *Energy & Fuels* 29 (2015) 6456–6464. <https://doi.org/10.1021/acs.energyfuels.5b01303>.
- [41] M. Israelsson, M. Seemann, H. Thunman, Assessment of the Solid-Phase Adsorption Method for Sampling Biomass-Derived Tar in Industrial Environments, *Energy & Fuels* 27 (2013) 7569–7578. <https://doi.org/10.1021/ef401893j>.

- [42] A. Larsson, M. Seemann, D. Neves, H. Thunman, Evaluation of Performance of Industrial-Scale Dual Fluidized Bed Gasifiers Using the Chalmers 2–4-MW_{th} Gasifier, *Energy & Fuels* 27 (2013) 6665–6680. <https://doi.org/10.1021/ef400981j>.
- [43] S. Pissot, T. Berdugo Vilches, J. Maric, I. Cañete Vela, H. Thunman, M. Seemann, Thermochemical Recycling of Automotive Shredder Residue by Chemical-Looping Gasification Using the Generated Ash as Oxygen Carrier, *Energy & Fuels* 33 (2019) 11552–11566. <https://doi.org/10.1021/acs.energyfuels.9b02607>.